Flexible and Printed Electronics

OPEN ACCESS

RECEIVED
3 October 2019

ACCEPTED FOR PUBLICATION
31 October 2019

PUBLISHED
9 January 2020

Original content from this work may be used under the terms of the Creative Commons Attribution 3.0 licence.

Any further distribution of this work must maintain attribution to the author(s) and the title of the work, journal citation and DOI.

PAPER

Scalable fabrication of organic solar cells based on non-fullerene acceptors

Anders S Gertsen[1], **Marcial Fernández Castro**[1], **Roar R Søndergaard** and **Jens W Andreasen**

Department of Energy Conversion and Storage, Technical University of Denmark, Frederiksborgvej 399, DK-4000 Roskilde, Denmark

[1] These authors contributed equally to the work.

E-mail: jewa@dtu.dk

Keywords: organic photovoltaics, scalable fabrication, printing and coating, non-fullerene acceptors, polymer solar cells

Abstract

Organic solar cells have recently experienced a substantial leap in power conversion efficiency, in part driven by formulations with new non-fullerene acceptors. This has brought the technology past the psychologically important mark of 15% efficiency for unscaled laboratory devices, and the results are stimulating another burst of research activity. Whether this will propel the technology into a viable commercial contender has yet to be determined, but to realize the potential of organic solar cells for utility scale application, fabrication using scalable processing techniques has to be demonstrated—otherwise, the passing of the 15% mark will eventually leave no more lasting impact than what the passing of the 10% mark did. Thus, addressing the scaling lag between the 15% cell efficiencies of lab-scale devices on rigid glass substrates fabricated using non-scalable techniques and the 7% efficiencies of scalably fabricated devices on flexible substrates is key. Here, we discuss the concept of scalability and give an account of the literature on non-fullerene acceptor devices fabricated with scalable methods and materials. On the basis of this, we identify three crucial focus points for overcoming the lab-to-fab challenge: (i) dual temperature control, i.e. simultaneous control of the ink and substrate temperatures during deposition, (ii) systematic *in situ* morphology studies of active layer inks with new, green solvent formulations during continuous deposition, and (iii) development of protocols for continuous solution processing of smooth, transparent interfacial layers with efficient charge transfer to the active layer. Combining these efforts and in general accompanying such studies with stability analyses and fabrication of large-area, scalably processed devices are believed to accelerate the relevance of organic solar cells for large-scale energy supply.

1. Broader context

Climate change is arguably one of the biggest challenges currently faced by human kind. Honouring the Paris Agreement and thus keeping the average global temperature rise in this century below 2 °C relative to pre-industrial levels demands an ambitious effort to replace fossil fuels with sustainable energy sources in our electricity production. Silicon solar cells are experiencing a rapid increase in worldwide installed capacity, but also new generations of solar cell technologies have the potential to reach maturity as a sustainable technology in the near future and thus to aid this transition. The key to the sustainability in terms of energy and materials use of these emerging technologies is scalability. Although silicon solar cell technologies have proven that upscaling fabrication also leads to significant cost reductions, their fabrication remains very energy consuming. Organic solar cells could prove to be a viable alternative with projected energy payback times of only fractions of those of silicon modules. Already now, organic solar cells are used for niche applications owing to their semi-transparency, flexibility, low weight, and possibilities of custom designs in terms of colors and shapes. In addition, utility scale competitiveness of organic solar cells with mature thin-film technologies is edging closer in current years with researchers pushing laboratory cell efficiencies beyond 15% using novel non-fullerene acceptor materials and several companies continuously improving large-scale fabrication; bridging these efforts and thus addressing the lab-to-fab challenge remains the most significant hurdle for the sustainable scalability of organic solar cells.

© 2020 The Author(s). Published by IOP Publishing Ltd

2. Introduction

Organic photovoltaics (OPVs) are often cited as one of the most promising third generation solar cell technologies because of their compatibility with solution processed roll-to-roll fabrication, enabling a fast and continuous fabrication [1–3]. Whereas the projected energy payback times of roll-to-roll fabricated OPVs are as short as weeks [4], at least an order of magnitude better than those of silicon technologies [5], the large-scale, grid-connected installations of OPVs continue to be halted by economical inferiority. In order to overcome this, improvements of especially stabilities, but also efficiencies, of flexible OPV modules are needed [6, 7]. However, properties that are beneficial for building integration such as low weight and partial transparency have given OPVs an advantage, and a number of companies are focusing on these alternative applications.

With the surpassing of the psychologically important 15% power conversion efficiency (PCE) mark for single junction cells earlier this year [8], it is clear that the field of OPVs is experiencing a revitalization which can mainly be attributed to the emergence of non-fullerene acceptor materials [9, 10]. The advantages of these over fullerene-based acceptor materials do not only comprise higher efficiencies, but also improved optical absorption and tunability as well as superior cell stabilities [11–16]. Combined with the recently reported low dependence of the PCE on active layer thicknesses and areas for high-efficiency systems [8, 17, 18], many prerequisites for the upscaling of organic solar cells are nearly fulfilled.

In accordance with previous endeavors related to fullerene-based OPVs [1, 19–23], we believe that it is paramount for the continued growth of the research field as well as a sustainable scaleup of the technology that the current focus on high PCEs and material development within fullerene-free OPVs is accompanied by:

(a) the use of roll-to-roll compatible or other scalable deposition methods in addition to spin coating,

(b) efficiencies of larger cells ($\geqslant$1 cm^2) or even modules alongside the small scale champion devices which are often only on the order of mm^2, and

(c) stability analyses.

If these parameters were to be consistently reported, it would enable a more concentrated effort towards addressing the lab-to-fab challenges (visualized in figure 1) and meeting the 10-10 targets for flexible organic solar cell modules of 10% efficiency and 10 years stability [1]. Held up against extensive economical analyses based on flexible OPV modules with 7% PCE and stabilities of 5–10 years that predict superior levelized costs of electricity compared to mature solar technologies such as e.g. crystalline silicon [7, 24], the 10-10 targets almost seem like a conservative estimate for sustainable scalability of organic solar cells. This further motivates overcoming the lab-to-fab challenges: in recent years, efficiencies well above 10% have consistently been reported for fullerene-free, spin-coated, small-area laboratory devices on glass substrates [17, 25–30], and 10% has also been reached using partly or fully scalable active layer deposition techniques (see section 3 for a discussion of scalability) [31, 32]. Even flexible devices with scalably deposited fullerene-free active layers are exhibiting efficiencies above 7% [33, 34], which, coupled with recent reports of 10 year lifetimes (extrapolated from 200 h stabilities) in fullerene-free, laboratory-scale devices by Du, Brabec *et al* [16], indicates that the 10-10 targets are within immediate reach.

The current limitations in upscaling of OPVs are complex and involve a series of challenges, including materials' compatibility, choice of non-toxic solvents, choice of compatible interface materials and, most importantly, stability and costs. Evaluating and seeking to overcome these limitations in devices processed using non-scalable deposition techniques such as spin-coating is inherently problematic, and they should instead be evaluated in the framework of fully scalably deposited OPVs. In this perspective, we review state-of-the-art fullerene-free, single junction OPV devices and the extent to which scalable techniques and materials are used in the fabrication. Aided by a discussion of the terminology related to the concept of scalability as it is used in connection with fabrication of organic solar cells, we aim to assess the potential of organic solar cells for sustainable scalability, to evaluate which material systems are the most promising for upscaling, and to suggest focus points for overcoming the lab-to-fab challenges currently faced. We note that a similar deserved attention is given to the closely related field of upscaling of perovskite solar cells in a recent publication, underlining the relevance of this challenge for third generation solar cells in general [35].

3. Scalability: a note on semantics

The word 'scalable' can generally be interpreted as the capability of a process to handle a larger workload without significantly compromising functionality and cost. However, formulating a clear cut definition of scalability in the context of organic solar cell fabrication is at best a very difficult task and not the purpose of this section. Instead, we seek a discussion and eventually a community-wide consensus on a terminology, allowing for a higher degree of transparency in the reporting of OPV devices. As a first iteration, and for categorizing fabrication processes reviewed in the

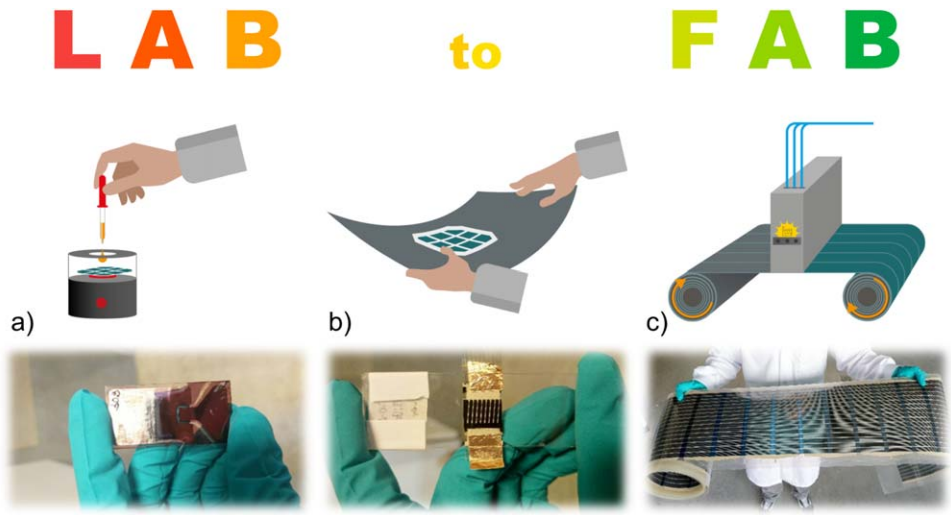

Figure 1. The lab-to-fab challenge: upscaling fabrication of organic solar cells from (a) lab-scale devices fabricated using non-scalable methods and materials on rigid substrates through (b) lab-scale devices fabricated using scalable methods and materials on flexible substrates to (c) large-scale, roll-to-roll fabrication on flexible substrates using fully scalable methods and materials.

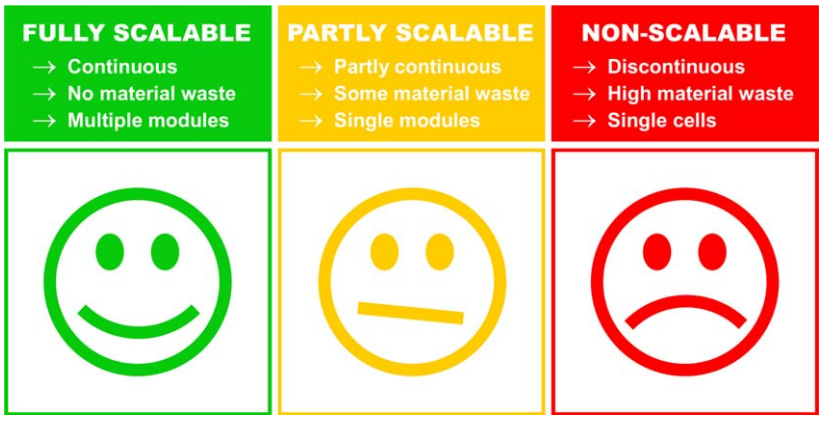

Figure 2. Classifications of deposition methods.

present article, we suggest the following three classifications (illustrated in figure 2).

(a) Fully scalable: high throughput deposition techniques that are directly compatible with continuous roll-to-roll setups and are linked to no material waste.

(b) Partly scalable: deposition techniques that can be made compatible with continuous roll-to-roll setups with some modifications and/or are linked to some material waste.

(c) Non-scalable: low throughput deposition techniques that are incompatible with continuous roll-to-roll setups and/or are linked to a high material waste.

These can be used to classify deposition techniques of both active layers and electrodes as well as interfacial layers such as hole- and electron-transport layers. The arguments for the placement of specific deposition techniques in these categories will be given in section 4 alongside descriptions of these.

Defining scalability of the actual active layers based on non-fullerene acceptors is yet more complex. A material can have properties that allow for the use of scalable deposition methods without being scalable itself, simply because the material synthesis or manufacture is too elaborate and thus too expensive to use in an upscaling process. In this context, we would like to highlight the recent work by Li *et al* on an industrial figure of merit for the cost potential of fullerene-free OPVs [36], an extension of previous work by Min *et al* from 2017 [23], which in turn is inspired by the work of Bundgaard *et al* from 2015 [37]. By taking the synthetic complexity of the donor and acceptor materials into account alongside the PCE and the photostability of a device, this industrial figure of merit, i-FoM,

allows for a quantitative comparison of viability for upscaling across different active layers and the resulting devices. The synthetic complexity reflects the number of synthetic steps, the yield, the isolation/purification process, and the number of hazardous chemicals used, and it is therefore indirectly a qualitative estimation of both cost and sustainability of the donor and acceptor materials, making it a strong indicative measure of the scalability of the active layer itself. Taking the current rapid development of increasingly complex donor polymers and non-fullerene acceptors into account [14, 38–40], we believe that this i-FoM value could serve as an important tool in the evaluation of their scalability going forward. This, however, should not stand alone when discussing the potential for upscaling fabrication, since it does not incorporate the scalability of the fabrication as discussed above.

It is important to underline that scalability encompasses more than what is related to deposition techniques and active layers. Especially broader economical considerations regarding materials, processing conditions, and solvents are important for sustainable scalability of organic solar cell modules, but also environmental concerns should be taken into account. A number of significant contributions to the discussion of OPV scalability in terms of these parameters have been published throughout the years in the form of economical analyses [6, 7], life-cycle assessments [6, 41–43] and analyses of energy payback times [4, 5]. Although indeed interesting, these analyses are outside of the scope of this work, and we thus refer the interested reader to the cited articles.

4. Deposition techniques

In order to discuss scalability from a device fabrication point of view, it is important to understand the general working principles of how the different layers are deposited. Traditionally, the focus in the field has been on varying the active layer deposition, but here we will also try to incorporate interfacial layer deposition as well as electrode deposition. Comprehensive reviews of the different deposition techniques themselves have been published elsewhere [1, 44, 45], and we will hence refrain from extensive descriptions in the present paper and instead emphasize the discussion of their individual applicability to large-scale fabrication setups.

4.1. Coating and printing

We will here distinguish between coating and printing techniques—the former are used to deposit continuous layers along the translational direction of the substrate without direct contact to the surface of this, whereas the latter often are associated with the possibility to perform complex patterning through direct contact with the surface of the substrate, e.g. via a stamp, through the use of masks, or through control of the flow as is the case for inkjet printing. Because of the ability of printing techniques to deposit well defined patterns, they are highly applicable for electrode deposition in semi-transparent devices, whereas coating techniques are most often used for active and interfacial layer deposition given their continuous nature and possibilities to control film thicknesses by varying flow rates and/or web speed. All scalable techniques mentioned in the below paragraphs are illustrated in figure 3.

Spin-coating ☹ Spin-coating is a thin-film deposition technique relying on the dispensing of a solution onto a rotating substrate. The centrifugal 'force' will distribute the dispensed solution across the substrate surface, and combined with simultaneous evaporation of the solvent(s), a uniform thin-film of the solute(s) is obtained. This technique allows for easy control of the thin-film thickness from tens of nanometers to several micrometers by varying the angular spin-speed (the thickness, d, is proportional to the inverse of the square root of the angular velocity, ω: $d \propto \frac{1}{\sqrt{\omega}}$) [44], which, coupled with the possibility of spin-coating on very small areas, provides a powerful lab-scale technique for testing wide ranges of processing parameters. However, there are significant drawbacks for large-scale implementations such as a high material waste (most of the dispensed material is slung off of the substrate and onto the walls of the spin-coater) and the lack of possibilities to engineer a continuous version of this. Although commercial implementations of spin-coating in e.g. the LED industry enables deposition on areas of up to 1 m^2, the inherent batch process nature of spin-coating combined with the high material waste has made us label it non-scalable (see section 3 and figure 2). Spin-coating is thus one of the only deposition techniques that can not be used in scalable fabrication of OPVs, however, it remains to be the most widely used technique in literature for active layer and interfacial layer deposition due to the low equipment requirements and easy operation. The many years of experience with spin-coating deposition and historically the record device efficiencies achieved are obviously also significant drivers for the widespread use of this technique.

Doctor-blading/blade coating 😐 Because of its minimal equipment requirements and easy transferability to a roll-to-roll setup (as knife coating, see below), doctor-blading is often employed as the first step towards a more scalable deposition of active layers compared to spin-coating. By depositing an ink directly onto a substrate and subsequently dragging a sharp knife or a blade across it at a fixed distance, a wet thin-film with a well-defined thickness is obtained (see figure 3(a)). The empirical relationship defining the dry thickness, d, of this film is given by $d = \frac{1}{2} g \frac{c}{\rho}$, where g is the distance between the blade and the substrate, c the ink concentration, and ρ the dry film density [44]. This technique is accompanied by some

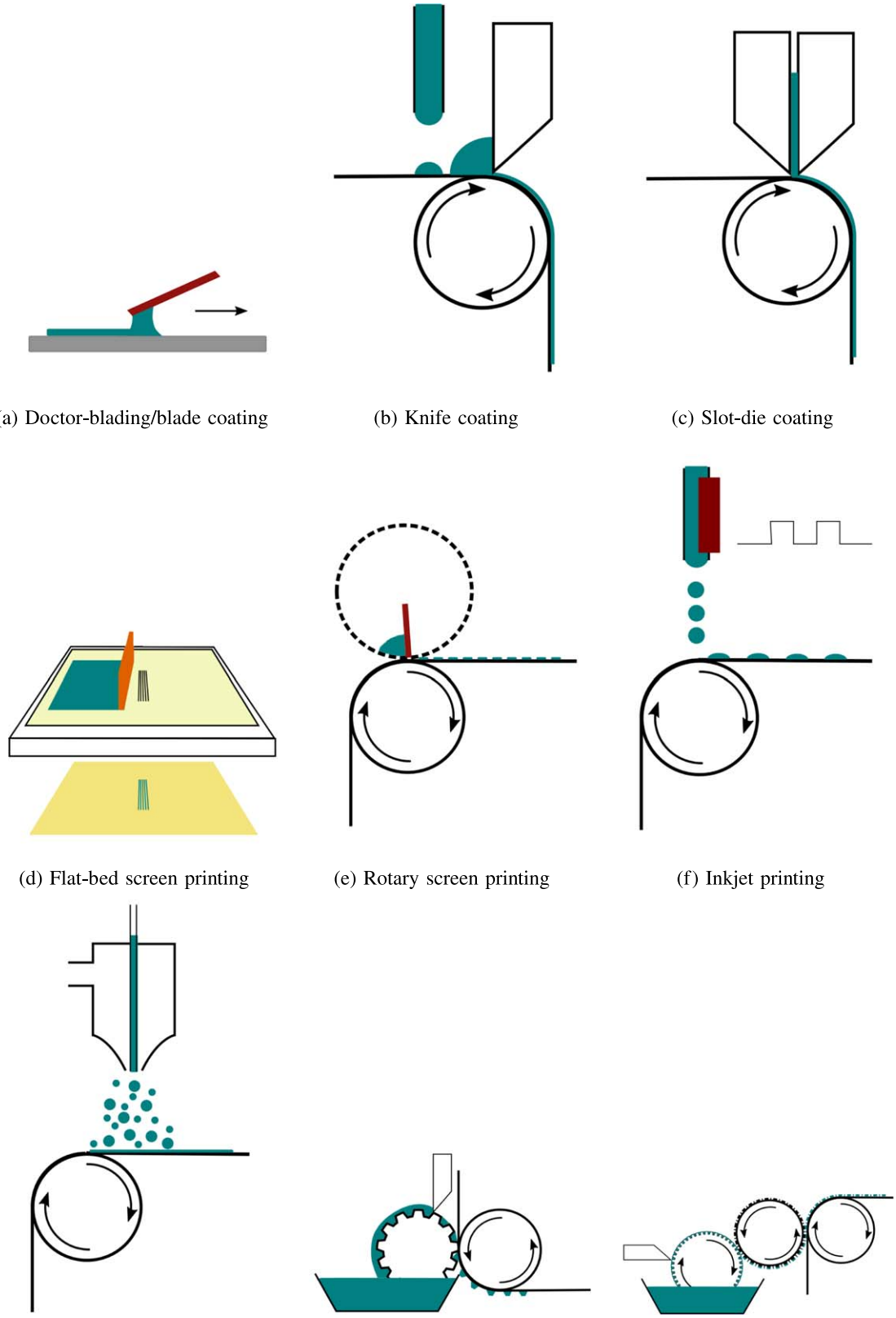

Figure 3. Deposition techniques that are partly or fully scalable (excluding vacuum techniques).

material waste, but with the possibility of obtaining coatings using only small amounts of material, it is a strong technique for laboratory scale testing. As the main limitation, formation of the thin-film using doctor-blading is slow compared to spin-coating, and volatile solvents combined with highly concentrated inks can thus lead to non-uniform films if aggregation has time to occur. In general, however, the longer

solvent evaporation times for doctor-blading are more comparable to the ones of other scalable deposition techniques.

A variation of the doctor-blading technique that deserves mentioning is the fluid-enhanced crystal engineering (FLUENCE) technique developed by Diao *et al* in 2013 [46]. By patterning the ink contact side of the blade with micropillar arrays, a flow-induced extensional strain facilitates increased crystallinity while simultaneously reducing domain sizes in all-polymer solar cells, in turn improving the device characteristics [47]. This principle could readily be applied to other deposition techniques described herein.

Knife coating ☺ Knife coating (or knife-over-edge coating) can be regarded as the continuous, roll-to-roll compatible analog to doctor-blading: an ink supplier gradually adds excess ink to a bath downstream of a knife, which controls the thickness of the wet film through its proximity to the substrate (see figure 3(b)). It is in essence a zero-dimensional technique, but the inherent lack of control of the width of the deposited layer can in part be solved by adding barriers to the ink bath and thus prohibit material waste, whereas also viscous inks allow for well-defined widths. The somewhat unknown width can furthermore complicate the calculation of the dry thickness (which is defined in a similar way to the one of doctor-blading, see above). In spite of knife coating being a fully scalable technique, the higher degree of patterning control in e.g. slot-die coating for active layer deposition will probably limit the applicability of knife coating in commercial setups.

Slot-die coating ☺ Slot-die coating enables a continuous, roll-to-roll compatible deposition of many varieties of inks and not least a one-dimensional control of coating patterns in the form of one or more stripes with well-defined widths. In slot-die coating, the ink is supplied via a pump to a slot-die coating head through which the ink is deposited onto a moving substrate (illustrated in figure 3(c)). There is practically almost no material waste, and the thickness of the dry film can thus easily be calculated as $d = \frac{c}{\rho}\frac{f}{vw}$, where f is the ink flow rate, v the coating velocity (i.e. the speed of the substrate or of the coating head), and w the width of the deposited ink [44].

The limitations of this technique are mainly related to the fluid dynamics defining the so-called coating window, i.e. the range of parameters for which a stable meniscus can be obtained, which relies on a range of properties, including flow rate, ink viscosity, distance of the coating head to the substrate, and coating velocity [48]. Slot-die coating is, however, a forgiving technique in the sense that a broad range of ink viscosities can be used and that its continuous nature allows for visual feedback while fine-tuning the above mentioned mechanical parameters until a stable meniscus is formed.

One of the drawbacks of conventional slot-die coating is the lack of temperature control in the tubing and the slot-die head. Compared to spin-coating, where the time from removal of the ink from a heat-bath to the deposition onto a heated substrate can be very short, the longer time needed for slot-die coating can cause problems for inks that undergo gelation below certain temperatures. This can in part be solved by hot slot-die coating in which the slot-die head is heated and connected to a thermo-couple, providing an extra temperature control in addition to substrate hot-plates—this deposition method has also proven to be very beneficial in terms of device efficiency as demonstrated in [33, 49].

Flat-bed screen printing 😐 Especially applicable for electrode deposition owing to its full two-dimensional patterning control, flat-bed screen printing employs a mask through which the ink is pushed into contact with the substrate using a moving squeegee (see figure 3(d)). Because of the nature of this process, there are significant limitations in terms of the ink properties: it should have a high viscosity to avoid deviations from the patterning and the solvent should have a low volatility to avoid evaporation causing concentration gradients and thus differences in dry film thickness along the squeegee translational direction. As the thickness of the deposited layer is defined by the mask thickness, screen printing techniques are mostly applicable when thick layers (wet layer thicknesses of 10–500 μm) are needed; [1] the dry thickness can be estimated by $d = k_p V_{\text{screen}} \frac{c}{\rho}$, where V_{screen} is the paste volume of the screen (theoretical volume of wet ink deposited per area of mask hole) and k_p is the ratio of this wet ink that practically remains on the substrate [44]. There is potentially only a low material waste connected to this technique, and with it being a sheet-to-sheet process easily applicable for large areas, it is labeled partly scalable. This, however, makes it a strong technique for laboratory scale testing, and with the possibility to adapt it to fully continuous roll-to-roll setups through rotary screen printing (see below), observations and results from flat-bed screen printing are readily transferable to fully scalable fabrication.

Rotary screen printing ☺ Developed as a roll-to-roll compatible version of screen printing, rotary screen printing makes use of a stationary squeegee around which a mask rotates (see figure 3(e)). An ink bath supplies material, which in a similar fashion to flat-bed screen printing is pushed through the holes in the mask onto the substrate to reproduce the pattern of the mask. The limitations related to the ink viscosity are the same as in flat-bed screen printing, but the volatility of the solvent can be higher, as the ink is somewhat protected from the surroundings inside the screen.

Inkjet printing 😐 Inkjet printing is a digitally controlled patterning technique known from standard printers. Using a nozzle with a piezoelectric stage or a thermal unit to eject ink droplets that are then

electrostatically charged and accelerated towards the substrate by an electric field, a digital pattern can be reproduced with high resolution and no material loss (illustrated in figure 3(f)). Although indeed attractive for niche applications where complex or varying patterning as well as aesthetics are necessary, the slow speeds, relative to slot-die coating, with which inkjet printing can coat large areas are a potential limitation for its use in large-scale fabrication of organic solar cells. We have hence, despite its apparent compatibility with a continuous roll-to-roll setup, labeled it partly scalable. Furthermore, restrictions on the ink to have a low viscosity to be able to form droplets can be prohibitive for inkjet printing of some layers. The thickness of a dry film deposited by inkjet printing can be calculated as $d = N_d V_d \frac{c}{\rho}$, where N_d is the number of droplets with volume V_d deposited per unit area [44].

Spray coating 😐 Like inkjet printing, spray coating relies on droplet formation of the ink. However, the requirements to the ink are more lenient compared to inkjet printing, facilitating the use of inks with a wide variety of rheologies and viscosities [50]. The most common spray coating technique is airbrush spray coating, where an aerosol is formed by forcing the ink out of the nozzle using a gas flow, usually N_2 (see figure 3(g)). Whereas inkjet printing is a two-dimensional patterning technique, spray coating is essentially zero-dimensional, although with the possibility of some one-dimensional control if variations in the stripe edges can be accepted. This sacrifice of patterning control, however, enables a significant speedup of the deposition, allowing for a more meaningful roll-to-roll implementation, but the relatively high surface roughness and thus the need for thicker layers to prevent pinholes can in practice lead to low-efficiency or even defect cells and in turn to material waste. We have therefore categorized this technique as only partly scalable despite its roll-to-roll compatibility.

Gravure printing 😊 Known from commercial printing, gravure printing is based on a gravure roller transferring ink from a bath via its engraved cavities to the substrate when pressed into contact (visualized in figure 3(h)). This allows for high speed processing and two-dimensional patterning in a continuous roll-to-roll setup with the shape and thickness of the obtained patterns defined by the engravings in the gravure roller. As the main limitation of gravure printing, the necessary optimization of the ink's surface tension should be mentioned, since factors such as the ink rheology and the pressure of the gravure roller on the substrate affect the quality of the print significantly [1].

Flexographic printing 😊 In flexographic printing, the ink is transferred from the bath via an anilox roller, which is a cylinder with ink-collecting micro-cavities, to the relief of a printing roller that then 'stamps' its pattern onto the substrate when pressed into contact (see figure 3(i)). Like for gravure printing, this allows for two-dimensional patterning control in continuous roll-to-roll setups, and the remaining advantages and limitations are very similar to this too.

4.2. Vacuum deposition

Previously, vacuum steps have been regarded as being non-compatible with large-scale fabrication of organic solar cells, and 'vacuum-free' has often been used in literature as a precondition for scalability [21, 44, 51–53]. We would, however, like to challenge that position with reference to the numerous commercial photovoltaic technologies incorporating vacuum deposition steps such as organic light emitting diodes and silicon solar cells. Furthermore, Heliatek has demonstrated with their HeliaFilm® pilot line in 2016 and later with a small-scale fabrication line that a full roll-to-roll setup in inert atmosphere and with several vacuum steps is indeed realizable and not least commercially promising [54]. Very recently, the group led by M Madsen at the University of Southern Denmark also demonstrated roll-to-roll vacuum sputtering using their in-house setup [55]. Vacuum steps are thus not prohibitive for the upscaling of the fabrication itself, and if the costs related to material use and processing conditions, amongst these high-temperature steps, can be kept down as indicated by the commercial nature of the HeliaFilm® project, vacuum- and inert steps are likely to be part of the future large-scale fabrication of organic solar cells because of the efficiency gains usually seen compared to solution processing in ambient conditions.

Thermal evaporation 😐 Also known as vapor deposition, thermal evaporation relies on resistive heating of an evaporation source, for example silver in the case of electrode deposition, under vacuum until a vapor pressure is reached and the evaporated silver is deposited on a substrate, forming a thin-film. Thermal evaporation allows for a precise control of the layer thickness and produces highly uniform layers, and patterning control is achievable through the use of shadow masks: for one-dimensional control, a stationary mask would be sufficient, whereas two-dimensional patterning in a continuous setup would demand a mask moving with the same speed as the substrate. The requirement of shadow masks for patterning control is, however, linked to a not insignificant material waste, but the material deposited on the shadow mask could potentially be recycled. Even though this is a significant challenge, especially in terms of economy when using expensive materials such as silver, we have in the evaluation of this deposition method chosen to put emphasis on the possibility to integrate it into a roll-to-roll setup for continuous deposition and thus labeled it partly scalable.

Sputtering 😐 In sputter deposition, material is eroded off of a target source, e.g. molybdenum, using, in most cases, argon plasma. The sputtered material will then deposit on the substrate to form a thin-film. The atmosphere in the sputtering chamber can be

tuned to need—for example in the case of MoO_x hole-transport layers, molybdenum atoms are sputtered in a controlled oxygen atmosphere to obtain a stoichiometrically desired MoO_x layer. Like for thermal evaporation, the uniformity of the deposited layer is high, and its thickness can be controlled with a very high precision down to single nanometres. The need for shadow masks poses problems identical to the ones for thermal evaporation, but it should be noted that the amount of material needed per area is usually significantly lower for vacuum deposition than for solution processing because of the homogeneity of the vacuum deposited layers.

5. Overview of scalably fabricated, fullerene-free OPVs from literature

The availability of equipment and especially the ease of use are important explanatory factors for the relatively few studies published on fully scalable fabrication of organic solar cells. However, as discussed above, techniques like blade coating and flat-bed screen printing are optimal for laboratory-scale optimization and readily transferable to continuous roll-to-roll setups, but whereas blade coating has recently been used routinely for active layer deposition, top electrodes and interfacial layers are still, almost exclusively, thermally evaporated.

Opposed to scalable deposition techniques, the use of non-fullerene acceptor materials is not a prerequisite for commercial fabrication of organic solar cells, but they have to a large extent simply out-competed fullerene acceptors. Fullerene acceptors have historically been widely used in the active layers of organic solar cells owing to their favorable properties such as high electron affinities, high electron mobilities, and easy solution processing [56]. However, the low-energy transitions in fullerenes are dipole forbidden owing to their high molecular symmetry, in turn leading to weak optical absorbance in the visible spectrum, which is a significant limitation for further improvements in the efficiencies of fullerene-based organic solar cells. The optical properties of non-fullerene acceptors can to a higher degree be tuned by chemically engineering their molecular structure. The most widely used design principle for small-molecule, non-fullerene acceptor materials is to utilize a conjugated internal acceptor–donor–acceptor structure in which two electron withdrawing units (internal acceptors) are separated by a central electron donating unit (internal donor) and potential bridging units [57, 58]. In this way, the low-energy transitions are red-shifted due to a promotion of charge-transfer states, in turn facilitating an optical absorption profile dominant in the red part of the visible spectrum, complimentary to most polymer donor materials, which absorb in the blue and green parts of the spectrum. A second way to achieve this is by employing polymeric, non-fullerene acceptor materials with internally alternating donor–acceptor structures [38, 59, 60], similarly facilitating low-energy charge-transfer absorptions. Like for the fullerene acceptors, high electron affinities of both small-molecule and polymer non-fullerene acceptors are obviously paramount, but the active layer processing conditions for which optimal microphase separation and domain purity occur to ensure high electron mobilities can vary greatly for the three types of acceptors and not least for different deposition techniques. These considerations will be discussed below.

Another important consideration for scalable processing relates to the device architecture. On flexible substrates, and especially in a roll-to-roll context, the inverted device architecture has proven to be the most practical given the available materials and processing methods. In particular, hole-transport layers have shown to be problematic in normal device architecture solar cells, as they have to be both highly transparent (all light has to pass through it to reach the active layer) and mechanically robust (being the first layer processed on top of the transparent electrode, it is subject to high stress). The commonly used materials like PEDOT:PSS and hole-conducting metal oxides have so far not proven processable in a way where these demands are fulfilled. On the other hand, the materials for electron-transport layers have not suffered from the same problems. Highly transparent materials like ZnO and TiO_x are routinely used and have proven themselves as good front materials in inverted architecture solar cells while simultaneously allowing the use of less transparent and less robust hole-transport materials such as the above mentioned at the back of the solar cell. The dominance of the inverted architecture, as will be obvious from the following sections, is thus predominately a consequence of the availability of suitable materials. If new hole-transport materials with the right properties are found, there is in principle no reason why normal architecture solar cells could not be used in the future.

Throughout the coming sections, we have highlighted groundbreaking works and their resulting devices in figures 4–8. The molecular structures of all donor polymers mentioned in these sections are shown in figure 9, of all non-fullerene acceptors in figure 10, and of all molecular interfacial layers in figure 11. The device parameters for all mentioned devices, including short-circuit currents, open-circuit voltages, and fill-factors (FF), as well as qualitative estimates of the scalability of the materials and deposition techniques are summarized in table 1. Further details regarding this table can be found in section 5.5.

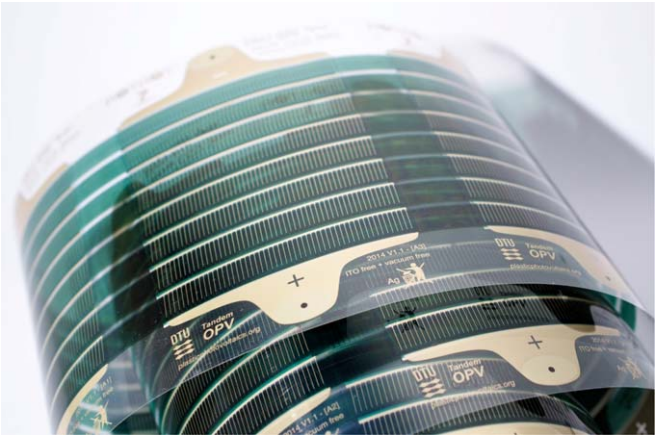

Figure 4. Flexible, ITO-free, vacuum-free OPV module fabricated using continuous roll-to-roll deposition techniques at the Technical University of Denmark.

5.1. Devices fabricated using solely roll-to-roll compatible deposition methods and no vacuum steps ☺

Only a few studies on fully roll-to-roll compatible, vacuum-free processing of non-fullerene systems have been reported. The first effort in this respect was published in 2013 by Liu *et al* [64], where they investigated the effect of upscaling small area devices on glass substrates with spin-coated active and interfacial layers and thermally evaporated electrodes to a complete roll-to-roll fabrication of large-area modules on flexible substrates. For the flexible devices, an inverted structure of indium tin oxide (ITO)/ZnO (NP)/PDI-DTT:PSBTBT/PEDOT:PSS/Ag was used; the polyethylene terephthalate (PET) substrate with ITO was purchased from a commercial supplier, the zinc oxide nanoparticles (ZnO(NP)), active layer (PDI-DTT:PSBTBT, see figures 9 and 10, respectively), and PEDOT:PSS (see figure 11) were slot-die coated, and the silver back electrode was deposited using a roll-to-roll integrated flat-bed screen printer. The average efficiencies of the resulting 4.2 cm^2 modules were 0.20%, a factor of three lower than the small-area, spin-coated devices on glass substrates, leaving notable room for improvement. The effect of the substrate (PET versus glass) was concluded to be a decisive factor, but probably most problematic for upscaling (disregarding the low performance) was the use of ITO. ITO has been shown to be both economically and environmentally critical, and in addition, the significant fraction of more than 80% of the embedded energy in similar modules stemming from the ITO coated PET posed a significant impediment for the projected energy payback times [6, 41].

This problematic use of ITO had already been addressed in fullerene-based OPVs at several occasions [65, 66], but the first study of roll-to-roll compatible processing of non-fullerene OPVs on flexible substrates without ITO was not published until 2014 by Chen *et al* [67]. This was additionally the first study looking to replace the fullerenes in the well-known model system P3HT:$PC_{61}BM$ (see figure 9) with small-molecule, non-fullerene acceptors in fully roll-to-roll processed OPVs, but the efficiencies reached were lower than 0.1%. However, the deposition techniques and the device structure used therein have been the dominant in literature since. The processing equipment was introduced in 2012 by Dam and Krebs, who reported a laboratory-scale coating/printing machine enabling the fully scalable processing of all layers in a stand-alone setup [68], and the device structure was introduced by Carlé *et al* later that year [69]. Using an inverted architecture of PET/Ag/PEDOT:PSS/ZnO(NP)/D:A/PEDOT:PSS/Ag (D: donor, A: acceptor), ITO- and vacuum-free devices could be realized, allowing for lab-scale assessment of new active layers in the context of large-scale fabrication. The processing is, in principle, straightforward: flexographic printing of a silver paste onto the PET substrate, slot-die coating of a ZnO nanoparticle solution, slot-die coating of a PEDOT:PSS ink, slot-die coating of an active layer ink, slot-die coating of a second PEDOT:PSS ink, and lastly flexographic printing of a silver paste as the top electrode. This also enables the use of pre-processed substrate foils with bottom electrodes and ZnO electron-transport layers already applied, making the testing of new systems simple as well as minimizing material waste.

The above procedure has been used in almost all studies of fully roll-to-roll compatible, non-fullerene acceptor OPVs published subsequently. In 2014, Cheng *et al* aimed to study the effects of the 1,8-diiodooctane (DIO) high boiling-point additive and to compare spin-coating on glass substrates with slot-die coating on flexible substrates in this type of setup for both fullerene-based systems and all-polymer systems [70]. Of the four combinations, the scalably processed, flexible, all-polymer cells with an

inverted Ag/PEDOT:PSS/ZnO(NP)/PBDTTT-C-T:PDIDTT/PEDOT:PSS/Ag structure (see figure 9 for structures; note that PDIDTT is only shown in here despite of its applicability as an acceptor too) showed the lowest average PCEs of 0.67% for 1 cm^2 devices. This was followed by a paper from the same authors in 2015 [11], using identical device structures and deposition techniques but with a small-molecule, non-fullerene acceptor (active layer: PBDTTT-C-T:DC-IDT2T, see figures 9 and 10). This led to a champion efficiency of 1.0% for a 1 cm^2 device, which was, however, still a factor of two lower than the $PC_{71}BM$ analog. On the other hand, the non-fullerene devices showed a far superior stability under continuous AM 1.5G illumination, maintaining more than 80% of their initial efficiency compared to the mere 50% of the fullerene-based device. This increased stability has later been shown to be a somewhat general characteristic for small-molecule, non-fullerene acceptors [12, 13, 16], giving them a significant advantage over fullerene acceptors for commercial viability.

The following year in 2016, Liu *et al* investigated devices based on the PTB7-Th:IEIC active layer (see figures 9 and 10 for molecular structures) [71]. With champion efficiencies of 6.31% in lab-scale, spin-coated devices on glass substrates with evaporated electrodes, it was a good candidate for upscaling to flexible devices deposited with fully scalable methods. They employed two types of flexible device structures on PET foil: an ITO-free one, namely Ag/PEDOT:PSS/ZnO(NP)/PTB7-Th:IEIC/PEDOT:PSS/Ag, and an ITO-containing one, namely ITO/ZnO(NP)/PTB7-Th:IEIC/PEDOT:PSS/Ag. As described above, the ITO-free devices were deposited using flexographic printing for the electrodes and slot-die coating for the remainder of the layers, whereas the PET/ITO foil was purchased and the remainder of the layers were processed as for the ITO-free devices. For the ITO-free devices, an average PCE of 1.60% with a champion efficiency of 1.79% was obtained for 1 cm^2 cells, whereas the ITO containing devices reached an average PCE of 2.05% and a champion efficiency of 2.26% for 0.7 cm^2 cells—all of these were slightly lower than their fullerene ($PC_{61}BM$) counterparts, but were at the time the highest reported efficiencies for flexible, non-fullerene devices. All cells in this study were suffering from low FF of around 35%, but the fullerene-free cells exhibited slightly higher FF than the fullerene cells, whereas the fullerene cells had significantly higher short-circuit currents. Stability tests were also performed, showing increased stability in the fullerene-free devices, in turn supporting the statement made in the previous paragraph.

Later that year, Brandt *et al* reported the only second work on combining P3HT and non-fullerene acceptors using roll-to-roll compatible processing [52]. Here, they investigated variations in absorption, crystallinity, and device performance based on the geometrical effects of three diketopyrrolopyrrole acceptors with different degrees of ground state planarity in a combined study between quantum chemical calculations, X-ray experiments, and device characterization. Obtaining only low efficiencies of 0.54% for the best roll-coated device (using the same device structure as described above), the most important conclusion drawn from this study was that the less crystalline system performed better in roll-coating, whereas the more crystalline system performed better in spin-coating. This underlines the need for *in situ* morphological studies of active layer deposition to probe the microstructure evolution during solvent evaporation [72–75].

For a couple of years after this, no studies on fully scalably fabricated, fullerene-free devices were published, but from 2016 onwards, significant effort has been put into synthesis of new and improved non-fullerene acceptors. The impressive efficiencies exceeding 10% reached in lab-scale devices using IDTBR small-molecule acceptors [13, 76–78] has, in 2018, motivated Strohm *et al* to produce P3HT:O-IDTBR modules using fully scalable deposition methods (see figure 10 for the structure of IDTBR) [61]. Although the modules were deposited on ITO coated glass substrates, which prohibits a true industrial fabrication as discussed above, we have chosen to include their work in this section because of their effort to upscale both the interfacial layers themselves and their deposition as well as the deposition of the top electrode. Using a device structure of ITO/ZnO(NP)/P3HT:O-IDTBR/PEDOT:PSS/AgNW (AgNW: silver nanowires), doctor-bladed 0.1 cm^2 cells with an average PCE of 5.25% and an average FF of 66.6% were fabricated using a solvent formulation of chlorobenzene with 5% 4-bromoanisole additive for the active layer processing. 59.5 cm^2 modules using the same device structure and processing conditions exhibited efficiencies of an impressive 5.0% (see figure 5), whereas exchanging doctor-blading for slot-die coating yielded modules with efficiencies of up to 4.4%. This system is thus indeed interesting for further studies on flexible, ITO-free substrates using true roll-to-roll deposition.

From this limited number of works on scalably fabricated, non-fullerene OPVs, it is clear that there is room for significant progress in the field. In line with our recommendations in the introduction, we urge an increased effort to demonstrate scalability both in terms of deposition techniques and materials. As will be evident from the below sections, promising material systems and solvent formulations as well as important considerations regarding interfacial layers

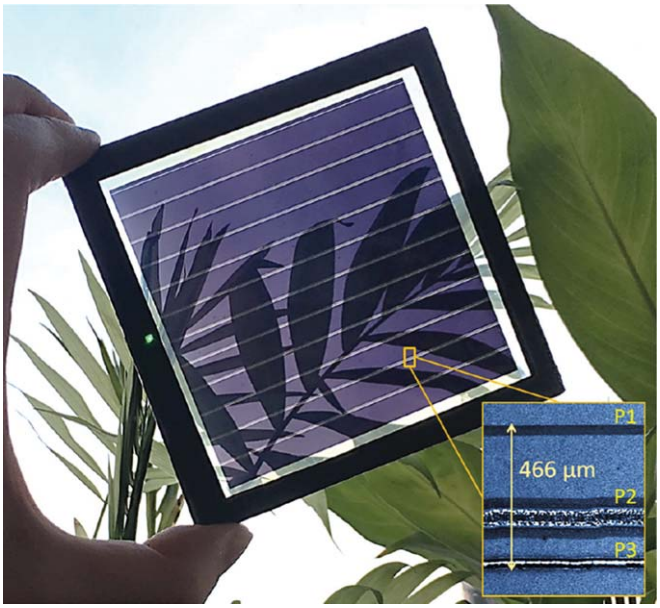

Figure 5. Rigid OPV module with P3HT:O-IDTBR active layers fabricated using roll-to-roll compatible deposition techniques by S Strohm, F Machui, and co-workers. Reproduced from [61] with permission from The Royal Society of Chemistry.

have been put forth, which, combined, will surely lead to advances for fully scalably fabricated OPVs.

5.2. Devices fabricated using solely roll-to-roll compatible deposition methods but vacuum steps 😐

As discussed in section 4.2, vacuum deposition techniques are likely to play a role in future large-scale fabrication of organic solar cells if the processing costs can be kept low; the techniques themselves are not incompatible with roll-to-roll setups. In this section, we will thus highlight studies utilizing vacuum deposition for the top electrodes and hole-transport layers but using continuous roll-to-roll deposition techniques for the active layers.

In 2017, Gu *et al* were the first to reach the 5% efficiency mark for fullerene-free organic solar cells using roll-to-roll deposition of the active layer [3]. In this study, different all-polymer active layers were studied in a PET/ITO/ZnO(NP)/D:A/MoO_3/Ag device structure, where the ZnO(NP) and active layers were slot-die coated onto a pre-produced PET/ITO foil in a custom-built roll-to-roll setup and the MoO_3 hole-transport layers as well as the silver top electrodes were thermally evaporated. Using sidechain engineering to control crystallinity, the two donor polymers PII2T and PII2T-PS (see figure 9) were synthesized and categorized as crystalline and low-crystalline, respectively, using grazing-incidence X-ray scattering. They were then paired with the two acceptor polymers PNDIT and PPDIT (see figure 10), similarly categorized as crystalline and low-crystalline, respectively. Spin-coated, lab-scale devices were then fabricated for each of the four pairs, showing that suppressing crystallinity led to higher device efficiencies caused by lower phase-separation sizes. The low-crystalline PII2T-PS:PPDIT pair was hence identified as the best candidate for upscaling, and cells were fabricated using the device structure described above. A small module with a combined area of 10 cm^2 was characterized, showing an average PCE of 4.1% with a champion PCE of 4.24% measured over 12 of the 0.12 cm^2 cells that were connected to form the 10 cm^2 module. With these impressive results in mind, they extended the study to encompass the PTB7-Th:PPDIE active layer (see figure 10 for molecular structures of PPDIE), which exhibited even lower crystallinity and phase-separation sizes than the PII2T-PS:PPDIT combination. The roll-to-roll coated devices based on this PTB7-Th:PPDIE active layer showed an average PCE of 5.0% with a champion PCE of 5.1%, at the time a record for flexible organic solar cells with continuously printed active layers. This work furthermore substantiates the findings of Brandt *et al* [52] described in the previous section, putting additional emphasis on the importance of morphological studies and showcasing the strength of developing design principles.

Very recently, in 2019, Na *et al* reported the current record efficiency of 7.11% for non-fullerene organic solar cells with roll-to-roll deposited active layers [33]. Extending their previous work on fullerene-based OPVs [49], their novel modification of a slot-die coater was used to investigate the effects of deposition temperature on device parameters of fullerene-free OPVs. By implementing a heating element in the slot-die head of a modified 3D printer,

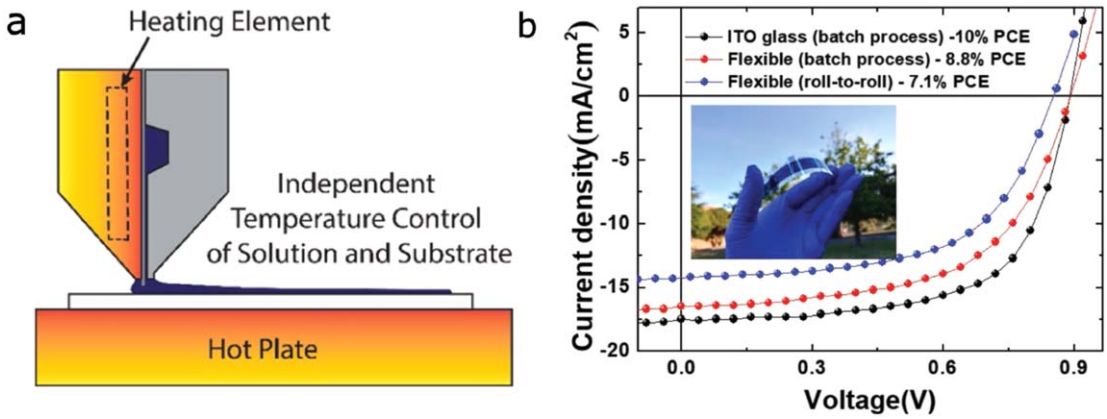

Figure 6. (a) Illustration of dual temperature control obtained in hot slot-die coating and (b) *J–V* characteristics of the different devices fabricated with slot-die coated active layers by S-I Na, D Vak, and co-workers. Reproduced from [33] with permission from WILEY-VCH Verlag GmbH & Co KGaA, Weinhim.

independent temperature control of the solution and the substrate was achieved (see figure 6(a)). Optimization showed large deviations of several percentage points in PCE with varying substrate temperature, whereas fixing the substrate at its optimum temperature of 120 °C and varying the slot-die head temperature showed a couple of percentage points difference with an optimum around 90 °C. They used an ITO/ZnO(NP)/PEIE/PBDB-T:ITIC/MoO_3/Ag device structure (see figures 9–11 for the structures) with pre-produced ITO-coated substrates, slot-die coating of the ZnO nanoparticles, the PEIE electron-transport layers, and the active layers, and thermal evaporation of MoO_3 and the silver top electrodes. PCEs of 10.0% on glass substrates with slot-die batch processing, 8.77% on PET substrates with slot-die batch processing, and 7.11% on PET substrates with full roll-to-roll, continuous slot-die processing were achieved for 0.07 cm^2 areas (see figure 6(b)). The latter is close to the current efficiency record for flexible OPV devices with roll-to-roll processed active layers of 7.32%, which was reached using an ITO/AZO:PEIE/PTB7:$PC_{71}BM$/MoO_3/Ag structure (AZO: aluminum-doped zinc oxide) in 2017 [34]. The discrepancy between the batch process and the roll-to-roll process for flexible substrates is explained by the physical contact between the coated film and the backside of the substrate on the rewinder roll, but this contact will be avoided in commercial roll-to-roll setups before the addition of the remainder of the layers or even before encapsulation. These results thus strongly indicate that dual temperature control can be key in overcoming the lab-to-fab challenge and realizing large-scale fabrication of flexible OPVs with high efficiencies.

5.3. Devices fabricated using partly scalable active layer deposition methods 😐

The vast majority of fully scalable deposition techniques are not straightforward to adopt in small-scale laboratory testing of costly material systems of which only small amounts are available. In particular, doctor-blading has been a popular choice as the first stepping stone towards scalable fabrication of organic solar cells because of its easy transferability to continuous processing. This makes it a strong technique for optimization of active layer solutions in terms of solvents, additives, material composition, and processing conditions in batch processes prior to upscaling. Hence, in this section, we will keep a principal focus on the active layers and review the most notable works using doctor-blading or other partly scalable techniques for the active layer deposition. Unless otherwise mentioned, ZnO(NP) electron-transport layers were spin-coated and MoO_3 hole-transport layers and Al or Ag top electrodes thermally evaporated for all reviewed devices below.

In the doctor-blading paragraph of section 4, we briefly touched upon the FLUENCE technique. In 2015, Diao *et al* used this variation of the doctor-blading technique to alter the morphology of all-polymer active layers [47]. It was found that the flow design with a microstructured blade increased the crystallinity of neat donor PII-tT-PS5 thin-films while concurrently reducing domain sizes in blend PII-tT-PS5:PPDIT thin-films (PPDIT is also denoted P(TP); see figures 9 and 10, respectively, for structures). Additionally, the surface roughness was also reduced significantly compared to regular, unstructured doctor-blading, in turn improving the reproducibility of device efficiencies. The combined effect of these properties led to a champion PCE of 3.2% in an inverted glass/ITO/ZnO(NP)/PII-tT-PS5:PPDIT/MoO_3/Al structure, the record efficiency for blade-coated, all-polymer organic solar cells at the time.

The following year in 2016, Ye *et al* reached a new record efficiency for blade-coated, all-polymer OPVs [79]. By doctor-blading a PBDT-TS1:PPDIODT active layer (see figures 9 and 10) in a green solvent, namely 2-methylanisole, in an inverted glass/ITO/ZnO(NP)/MoO_3/Al architecture, a champion PCE of 5.21% was achieved. This was one of the earlier efforts to replace the halogenated solvents regularly used for a green solvent, allowing for a more environmentally friendly

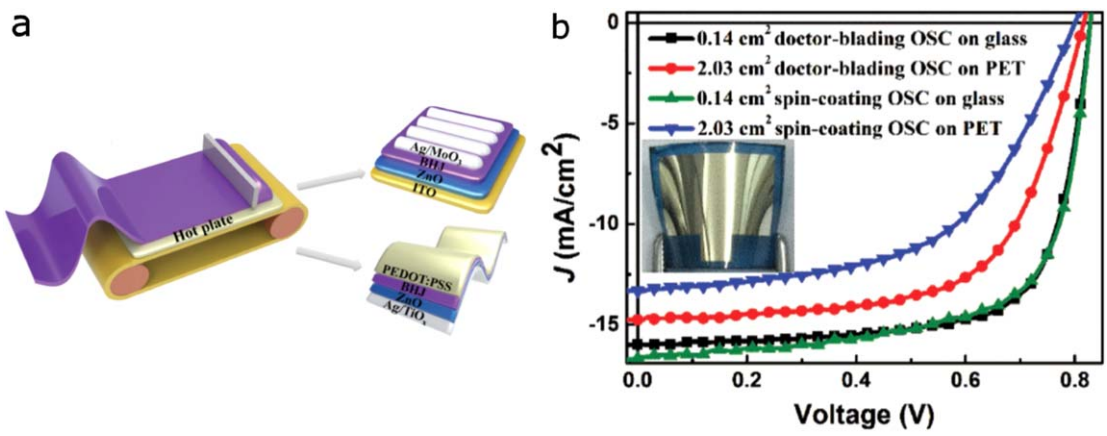

Figure 7. (a) Fabrication of rigid and flexible devices and their corresponding architectures with blade-coated active layers and (b) comparison of *J–V* characteristics of small- and large-area devices fabricated with spin-coated and blade-coated active layers by Y Lin, F Liu, F Zhang, L Hou, and co-workers. Reproduced from [62] with permission from WILEY-VCH Verlag GmbH & Co KGaA, Weinhim.

processing, which is particularly desirable for large-scale fabrication. More recently in 2019, Lin *et al* also focused on the use of non-halogenated solvents to control the morphology of all-polymer OPVs based on PTzBI:N2200 active layers (see figures 9 and 10, respectively, for structures) [80]. Using 2-methyltetrahydrofuran as the processing solvent, a champion PCE of 8.36% was achieved, whereas devices processed from chlorobenzene only reached 2.92% (both in glass/ITO/ZnO(NP)/D:A/MoO_3/Al inverted structures). This significant difference underlines the importance of exploring alternative—and preferably green—solvent formulations.

Moving to small-molecule acceptors, the ITIC non-fullerene acceptor and derivatives hereof have dominated the scene of blade-coated devices since late 2017. In December, Zhao *et al* investigated a methylated ITIC derivative, IT-M, in conjunction with the polymeric donor PBTA-TF (see figures 9 and 10) processed in green solvent formulations [81]. By comparing spin-coating and blade-coating of this active layer using both a low-boiling point solvent blend, namely tetrahydrofuran/isopropanol, and a high-boiling point solvent blend, namely *o*-xylene/1-phenylnaphthalene, it was found that the spin-coated devices performed slightly better when processed from the high-boiling point blend, whereas the blade-coated devices performed significantly better when processed from the low-boiling point blend. For these tetrahydrofuran/isopropanol processed, blade-coated devices, a record PCE of 11.7% was obtained in a conventional glass/ITO/PEDOT:PSS/D:A/PFN-Br/Al architecture (see figure 11 for PFN-Br structure) and 11.3% in an inverted glass/ITO/ZnO(NP)/D:A/MoO_3/Al architecture, both for 0.04 cm^2 devices. Impressively, large-area conventional devices of 1.0 cm^2 maintained a high efficiency of 10.6%, showing great promise for both this material system and the tetrahydrofuran/isopropanol solvent formulation for blade-coating.

In January 2018, Ye *et al* also investigated IT-M in an active layer with the FTAZ donor (see figure 9) similarly using a conventional glass/ITO/PEDOT:PSS/D:A/PFN-Br/Al architecture [31]. Once more, chlorobenzene processing, even with additives, was shown to be inferior to processing in additive-free, non-halogenated solvents, exemplified by pure toluene yielding a champion PCE of 11.0% for a 0.07 cm^2 cell, close to the above mentioned record at the time for blade-coated OPVs. For an area of 0.56 cm^2, an impressive PCE of 9.80% was reached, and with a dark stability of 85% of the initial PCE after 1000 hours in nitrogen atmosphere as well as only minimal FF reductions with longer annealing times at 150 °C, the morphological stability of this material system shows promise for adoption to commercial fabrication.

Simultaneously in January 2018, Lin *et al* published their efforts on doctor-blading flexible, large-area devices based on ITIC [62]. In a comparative study, they investigated the difference of spin-coated and blade-coated active layers as well as that of rigid substrates and flexible substrates (see figure 7). In addition, they worked with ITO-free PET for the flexible substrates, yielding the overall most scalable cells reviewed in this section. Starting from the glass substrates, doctor-blading the active layer in an ITO/ZnO(NP)/PTB7-Th:ITIC/MoO_3/Ag inverted structure, a champion PCE of 9.54% was achieved, slightly higher than the 9.31% of the spin-coated analog. For the flexible substrates, this difference was more pronounced with a champion PCE of 7.60% for doctor-blading and 5.86% for spin-coating in an inverted Ag/TiO_x/PTB7-Th:ITIC/PEDOT:PSS devices with large areas of 2.03 cm^2—the former 7.60% a record for large-area, flexible, ITO-free, non-fullerene OPVs with blade-coated active layers.

Later in 2018, Zhang *et al*, investigated the dependence of device characteristics on DIO additive content in chlorobenzene active layer processing solution for spin- and blade-coated glass/ITO/ZnO(NP)/PBDB-T:ITIC/MoO_3/Al cells [32]. Historically, DIO has been

key to achieving high efficiencies in devices deposited from halogenated solutions, but the difficulty of removing residual DIO content due to its high boiling-point has been shown to lead to accelerated morphology evolution [82] and degradation of device performance caused by iodine radicals formed under irradiation [83]. Using processing solvent formulations not dependent on DIO additives, as in the above described work of Ye *et al* [31], is thus the most obvious solution, although decreasing the DIO content would also be a step in the right direction. In the work mentioned in this paragraph by Zhang *et al* [32], it was found that blade-coated devices exhibited an optimum PCE of 10.0% for a DIO content of 0.25%, whereas the optimum PCE of 9.41% for spin-coated devices was achieved for a DIO content of 1.00%. This was reflected in the stability studies of unencapsulated devices, where the blade-coated cells with 0.25% DIO outperformed the spin-coated with 1.00% DIO on all parameters, both under illumination in ambient and in the dark under nitrogen atmosphere, indicating that both of the discussed degradation pathways were indeed relevant. These findings motivate morphological studies on residual additive content in dry OPV thin-films and in particular studies on alternative, additive-free processing solutions.

Jumping to 2019, Ji *et al* set out to investigate and optimize the surface morphology of ZnO electron-transport layers, leading to some of the highest efficiencies both for blade-coated OPVs in general of 12.88% for 0.12 cm^2 cells and for blade-coated, fullerene-free, large-area (>1 cm^2) OPVs of 9.22% for 1.04 cm^2 cells [84]. Two different solutions of zinc oxide nanoparticles were prepared and used in the inverted glass/ITO/ZnO(NP)/PBDB-T:IT-4F/MoO_3/Al devices (see figure 10 for IT-4F structure): one in acetone (A-ZnO) and one in methanol (M-ZnO). Scanning electron microscopy images revealed inhomogeneities and voids in pristine ZnO films spin-coated from acetone, whereas the methanol processed films exhibited compactness and an increased homogeneity. Additionally, atomic force microscopy showed a higher surface roughness for A-ZnO than for M-ZnO, which was ascribed to the faster drying process of the former ink. For devices of the above structure, the M-ZnO electron-transport layers yielded slightly better device performances than the A-ZnO layers when spin-coating the PBDB-T:IT-4F active layers (champion PCEs of 12.81% and 12.40% for 0.12 cm^2 devices, respectively), whereas this improvement was more pronounced when blade-coating the active layers (champion PCEs of 12.88% and 11.74% for 0.12 cm^2 devices, respectively). The performance disparity was hypothesized to originate from a change in interface charge transport properties between the active layer and the ZnO layers induced by the different surface morphologies of these, motivating further studies of this.

Very recently, Pascual-San-José *et al* published an elaborate study on blade-coated P3HT:NFA devices with a range of non-fullerene acceptors in an inverted glass/ITO/ZnO(NP)/D:A/MoO_3/Ag architecture [85]. Only the active layer deposition and the deposition of the ZnO(NP) electron-transport layer were, however, sought upscaled, and with an optimized efficiency of 5.6% for a P3HT:O-IDTBR active layer, the upscaling effort by Strohm *et al* [61] described in the above section 5.1 remains a stronger contribution on this specific system in terms of scalable fabrication. The strength of the study by E Pascual-San-José M Campoy-Quiles, and co-workers is, however, that they devise a high-troughput screening method incorporating variable speed blade-coating, enabling active layer thickness gradients, as well as a Kofler bench, enabling annealing temperature gradients. This continuous change of processing parameters allowed for the fabrication of more than a thousand devices of area 8 mm^2. In addition, an exemplary stability study was performed on P3HT:O-IDTBR devices, yielding the dependence of efficiency on encapsulation and active layer thicknesses. A degradation to 80% of initial performance was linearly extrapolated to >5 years for encapsulated devices with thin (80 nm) active layers, as compared to 8300 h for encapsulated devices with thick (250 nm) active layers, substantially longer than the 700 h and 120 h, respectively, for the corresponding unencapsulated devices (all based on measurements up to 3000 h). Interestingly, light-beam induced-current measurements suggested that P3HT suffered from a lower degradation rate than O-IDTBR, meaning that further optimization of IDTBR microphases could lead to better stabilities.

As a last work in this section, the 2019 study by D Corzo, D. Baran, *et al* on digital inkjet printed active layers deserves mentioning [63]. Using the P3HT:O-IDTBR material system also mentioned in section 5.1, inverted devices with a glass/ITO/ZnO(NP)/P3HT:O-IDTBR/MoO_3/Ag architecture were fabricated. By optimizing the rheologies of the ink formulations with respect to solvents and concentrations, a champion PCE of 6.47% for a 0.1 cm^2 cell was obtained for a homogeneous, inkjet printed active layer processed from a 1,2-dichlorobenzene solution. Increasing the active area to 2 cm^2 yielded only a small drop in device performance, sustaining a PCE of 6.00% (see figure 8(a)). In order to illustrate the possibility of full two-dimensional patterning using inkjet printing, a 2.2 cm^2 device in the shape of a marine turtle was fabricated with an efficiency of 4.76% (depicted in the inset of figure 8(b)), creatively demonstrating how versatile OPV custom designs can be.

The works highlighted above contribute with important observations on the path towards upscaling organic solar cell fabrication. First of all, the use of green, non-halogenated solvents are not only beneficial for the performance of fullerene-free OPVs deposited with scalable methods, but also for the device stability due to the elimination of the need for processing additives—and not least for the environmental friendliness of the fabrication itself. Secondly, and strongly linked to the first point, the volatilities of the solvents used during deposition of the active layers

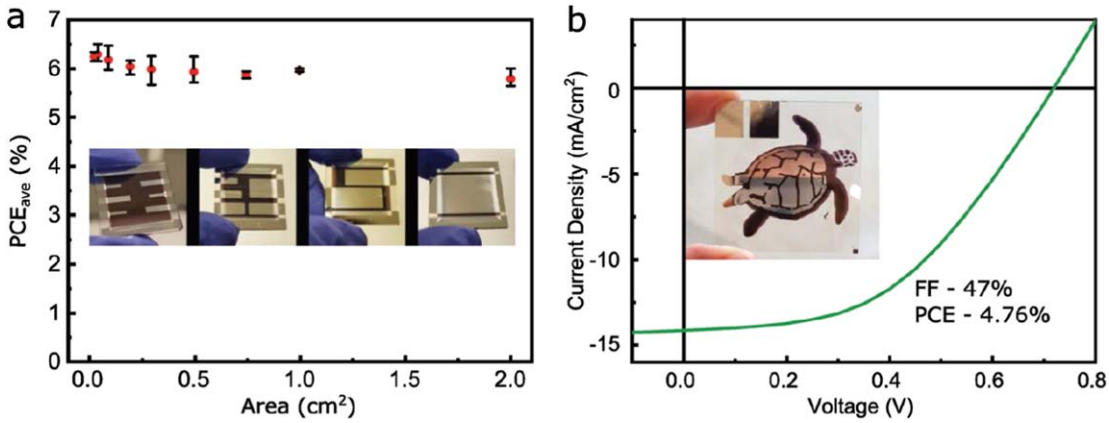

Figure 8. (a) The average efficiency of P3HT:O-IDTBR devices as a function of device area and (b) $J-V$ characteristics of an inkjet printed device in the shape of a marine turtle. Reproduced from [63] with permission from WILEY-VCH Verlag GmbH & Co. KGaA, Weinhim.

are crucial. Depending on the miscibility and crystallinity of the donor: acceptor couples, tuning the boiling-point of the solvent formulations is probably necessary to close the efficiency gap seen between spin-coated and scalably deposited active layers, as the slower evaporation times for techniques like blade-coating and slot-die coating could lead to unfavorable aggregation. This calls for more systematic solvent studies and preferably *in situ* morphological studies refining the, predominantly phenomenological, hypotheses based on indirect observations. Finally, we should strive to improve the smoothness of interfacial layers to promote charge transport between these and the active layers through altering the processing solvent formulations that are optimized for spin-coated fullerene devices. Surface morphology studies of slot-die coated interfacial layers processed from different solvents could hence provide essential insight into what seems to be a significant pathway for performance losses when upscaling deposition methods, especially when combined with studies of the interface between these and the active layer components.

5.4. Promising material systems for upscaling

The absence in literature of ITO-, vacuum-, and fullerene-free devices on flexible substrates fabricated using solely fully scalable deposition techniques with efficiencies of more than 2% underlines the need for a concentrated effort towards this goal. Most material systems presented in sections 5.2 and 5.3 show great promise for adoption to fully scalable fabrication, and in addition to these, a number of recent record-breaking lab-scale systems fabricated solely using spin-coating and vacuum deposition deserve mentioning. In this section, we will thus review selected works with donor: acceptor pairs that have, as of now, not been used in devices with scalably deposited active layers.

Already in the first months, 2019 proved to be an extraordinary year for organic solar cells, particularly fueled by the synthesis of a novel non-fullerene acceptor by the name of BTPTT-4F (also denoted Y6; see figure 10 for structure) [8]. First, Yuan *et al* reported this synthesis and demonstrated, at the time, record device efficiencies for single-junction OPVs of up to 15.7% (certified to 14.9%) for lab-scale cells with spin-coated PBDB-TF: BTPTT-4F active layers (PBDB-TF is also denoted PM6; see figure 9 for structure) [8]. Using both a conventional device architecture of glass/ITO/PEDOT:PSS/PBDB-TF:BTPTT-4F/PDINO/Al (see figure 11 for PDINO structure) and an inverted device architecture of glass/ITO/ZnO(NP)/PBDB-TF:BTPTT-4F/MoO_3/Ag, average PCEs of 15.6% and 15.5%, respectively, both with champion PCEs of 15.7%, were reached for 0.07 cm^2 cells. This equally high performance in inverted architectures is crucial, because the inverted structure significantly improves the long-term stability in ambient conditions relative to conventional architectures [86], which is a prerequisite for sustainable scalability of organic solar cells. Although their following studies on conventional architectures were not carried out for inverted architectures, they showed interesting tendencies. First of all, it was found that increasing the active layer thickness did not hamper the device efficiencies significantly: going from 150 to 300 nm yielded a two percentage point drop in champion PCE from 15.7% to 13.6%. Although the open-circuit voltages and the short-circuit currents remained largely unaffected by the increased thickness, the FF went down from 74.8% to 62.3% and was thus the main reason for the efficiency drop. Most notable, however, was the impressive performance of additive-free, as-cast devices: using no annealing steps after deposition, an average PCE of 15.2% was obtained, showcasing the stability of this material system with different processing conditions.

Shortly after, Fan *et al* reported the current efficiency record for single-junction OPVs of 16.0%, also using the BTPTT-4F non-fullerene acceptor [87]. A conventional architecture of glass/ITO/PEDOT:PSS/P2F-EHp:BTPTT-4F/PFNDI-Br/Ag was employed (structures for P2F-EHp and PFNDI-Br can be found in figures 9 and 11, respectively), leading to PCEs of 11.1% for additive-free, as-cast devices and, as mentioned, the record 16.0% using devices processed with

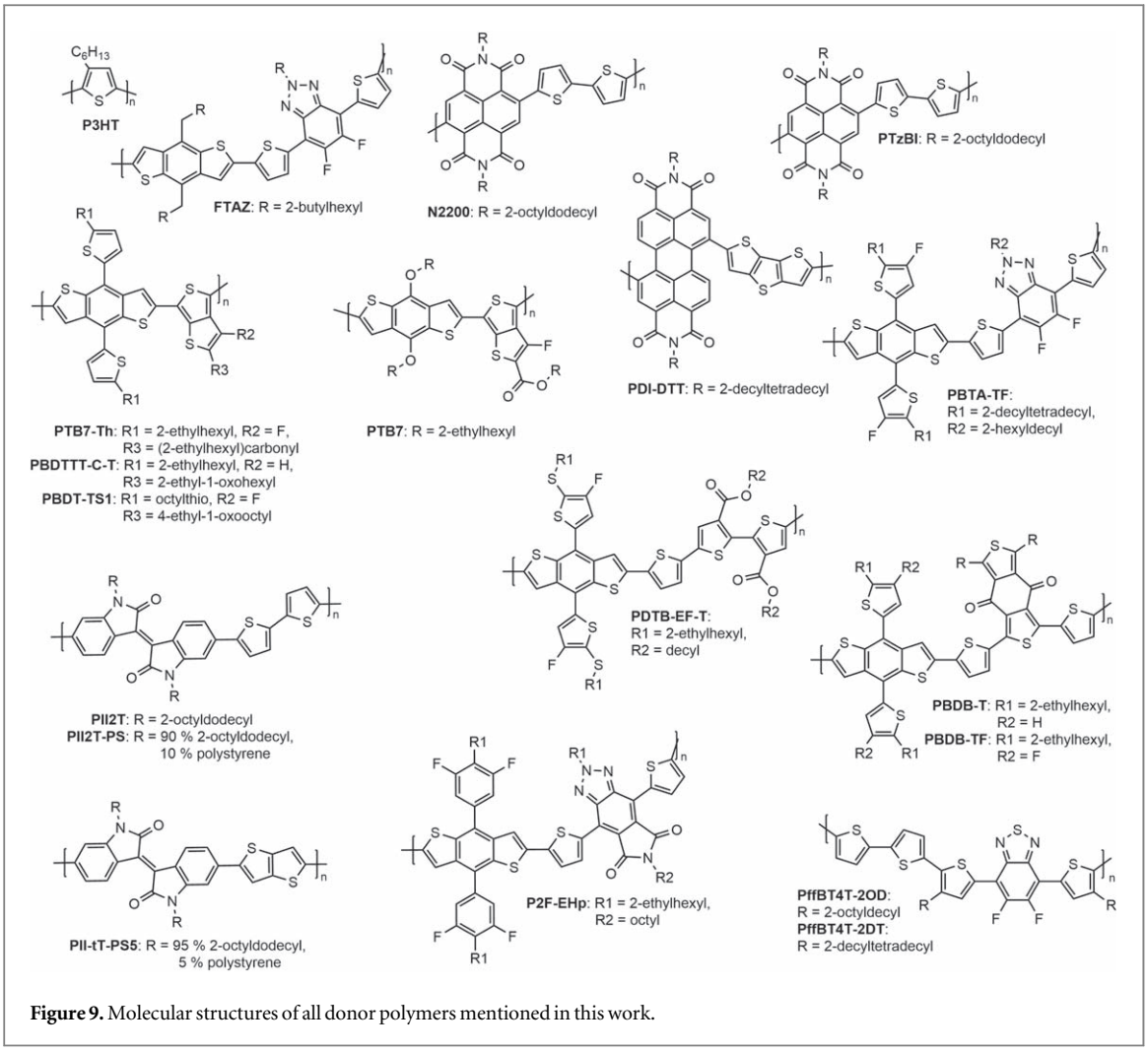

Figure 9. Molecular structures of all donor polymers mentioned in this work.

a relative amount of 1% dibenzylether solvent additive. Inverted devices were also fabricated, leading to a champion PCE of 13.1% for glass/ITO/ZnO(NP)/P2F-EHp:BTPTT-4F/MoO_3/Ag cells, also processed with 1% dibenzylether. BTPTT-4F is thus indeed a promising non-fullerene acceptor that holds a great potential for application in upscaled systems.

In the previous section 5.1, the IDTBR non-fullerene acceptor was introduced, and cells and modules utilizing this in conjunction with P3HT donor polymers were reviewed. However, coupling the IDTBR acceptor with PffBT4T derivatives (see figure 9) has consistently yielded efficiencies of around 10%–11% in lab-scale devices [13, 76, 78], making this an attractive material system for testing in scalable fabrication when taking the favorable properties into account such as negligible burn-in efficiency losses [13], high open-circuit voltages above 1 V [76], and high reproducibility and lifetime when processed in green solvents (non-halogenated hydrocarbons) [78].

Finally, the ITIC family of small-molecule acceptors should be mentioned. As reviewed in section 5.2, the PBDB-T:ITIC system has already proven to be very well performing in slot-die coated layers, and coupled with the impressive results obtained for blade-coated layers as presented in section 5.3, it is clearly indicated that variations of this material system hold great potential for scalably processed OPVs. Furthermore, in 2018, the efficiency record for single-junction organic solar cells was held by a cell incorporating an active layer based on the flourinated IT-4F acceptor, namely PDTB-EF-T:IT-4F (see figure 9 for donor structure). In a glass/ITO/ZnO(NP)/PDTB-EF-T:IT-4F/MoO_3/Ag inverted structure, average PCEs of 14.0% were obtained with a champion PCE of 14.2% (certified to 13.9%) and an impressive FF of 76% [29], further profiling ITIC derivatives as some of the best acceptor candidates for future fullerene-free OPVs.

With these high-efficiency material systems in mind, alongside the considerations regarding processing when going from spin-coating to scalable deposition described in the previous section, it seems that the active layers will not be the limiting factors for large-scale fabrication of organic solar cells with efficiencies of 10% or more. Knowing that the intrinsic charge transport and -transfer properties of the polymer donors and non-fullerene acceptors indeed facilitate high-efficiency active layers, focus can be put on optimizing the morphology of slot-die coated inks through systematic studies of processing conditions,

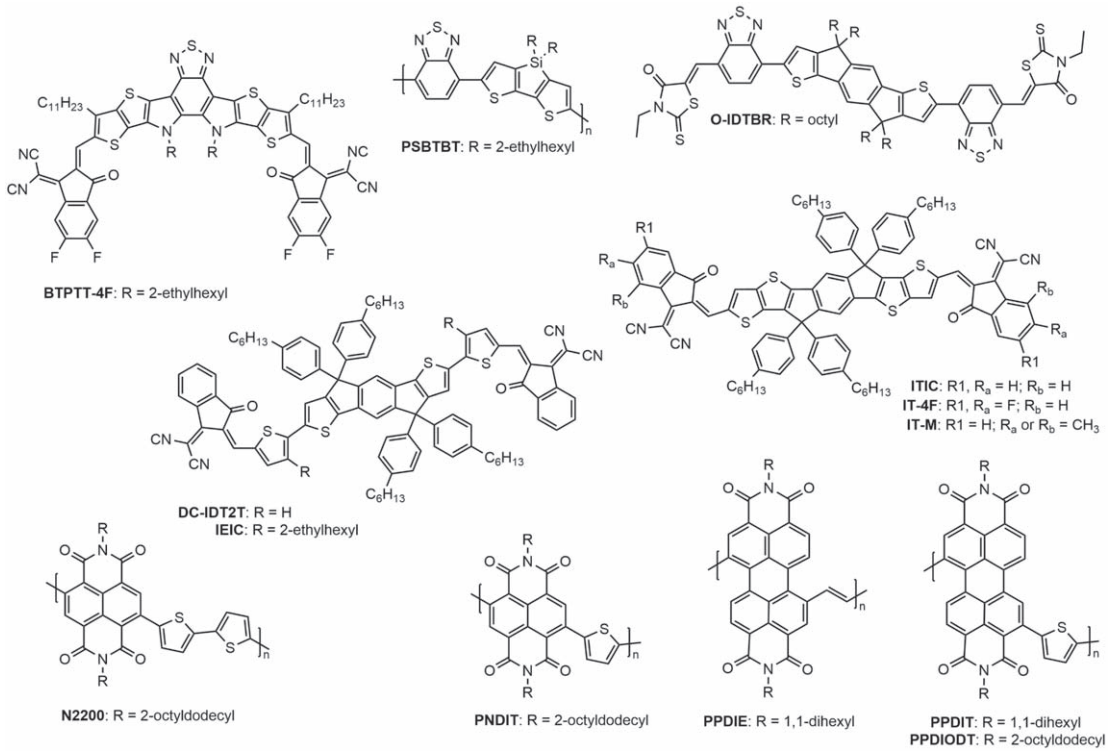

Figure 10. Molecular structures of all non-fullerene acceptors mentioned in this work.

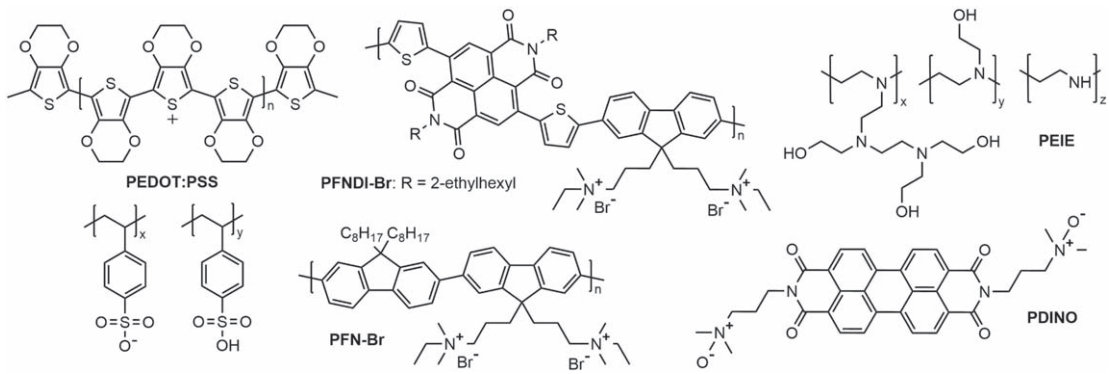

Figure 11. Structures of all molecular interfacial layer materials mentioned in this work.

including dual temperature-control and solvent formulations. Furthermore, and probably equally importantly, the interfaces between the active layers and the electron- and hole-transport layers should be optimized with regards to smoothness using scalable, continuous deposition techniques.

5.5. Summary of the reviewed devices

In table 1, the deposition methods and characteristics of all devices reviewed in the above sections 5.1–5.4 are listed. This includes the donor and non-fullerene acceptor (D:A) materials, the deposition method of the active layer, the processing solvent formulation, the substrate material(s), the deposition method of the top electrode, the device areas, and their corresponding champion PCEs, FF, open-circuit voltages (V_{oc}), and short-circuit currents (J_{sc}).

The deposition methods are classified using the smiley-model presented in section 3 by their colors green, yellow, or red to provide a quick overview. A similar classification is used for the processing solvents: halogenated solvents are marked with yellow and non-halogenated solvents with green as a representation of their environmental friendliness. Correspondingly, the substrates are marked with red for rigid glass substrates, yellow for PET substrates with

Table 1. Overview of the materials and deposition methods used for the reviewed devices alongside their performance characteristics.

D:A materials (see figures 9–10)	Active layer deposition	Solvent(s)	Substrate	Top electrode deposition	Device area (cm^2)	PCE_{max} (%)	FF (%)	V_{oc} (V)	J_{sc} (mA cm^{-2})	Year	References
PDI-DTT:PSBTBT	Slot-die, R2R	CB:CN	PET/ITO	Flat-bed, R2R	4.20	0.20	28.9	0.37	1.9	2013	[61]
P3HT:DPP(BT-N_3)$_2$	Slot-die	CF	PET	Flexographic	1.00	0.07	37.6	0.53	0.3	2014	[64]
PBDTTT-C-T:PPDIDTT	Slot-die	CB:DIO	PET	Flexographic	1.00	0.73	42.5	0.63	2.5	2014	[67]
PBDTTT-C-T:DC-IDT2T	Slot-die	CB	PET	Flexographic	1.00	1.02	40.1	0.80	3.1	2015	[11]
PTB7-Th:IEIC	Slot-die	*o*-DCB	PET/ITO	Flexographic	0.70	2.26	36.7	0.90	5.4	2016	[68]
	Slot-die	*o*-DCB	PET	Flexographic	1.00	1.79	35.2	0.94	6.9		
P3HT:Ph(DPP)$_3$	Slot-die	CF	PET	Flexographic	1.00	0.54	35.8	0.82	1.5	2016	[52]
P3HT:O-IDTBR	Doctor-blading	CB:BrA	Glass/ITO	Doctor-blading	0.10	5.25[a]	66.6	0.70	11.3	2018	[76]
	Doctor-blading	CB:BrA	Glass/ITO	Doctor-blading	59.5	5.00	64.9	0.71	10.9		
	Slot-die	CB:BrA	Glass/ITO	Slot-die	59.5	4.40	64.9	0.70	9.8		
PII2T-PS:PPDIT	Slot-die, R2R	CB	PET/ITO	Thermal evap.	10.0[a]	4.24	45.0	0.99	9.6	2017	[3]
PTB7-Th:PPDIE	Slot-die, R2R	CB	PET/ITO	Thermal evap.	10.0[a]	5.10	50.0	0.64	15.5	2017	[3]
PBDB-T:ITIC	Slot-die	*o*-DCB	Glass/ITO	Thermal evap.	0.07	10.00	64.9	0.88	17.5	2019	[33]
	Slot-die	*o*-DCB	PET/ITO	Thermal evap.	0.07	8.77	58.6	0.88	17.0		
	Slot-die, R2R	*o*-DCB	PET/ITO	Thermal evap.	0.07	7.11	58.1	0.86	14.2		
PII-tT-PS5:PPDIT	Doctor-blading	CB	Glass/ITO	Thermal evap.	0.04	3.20	46.0	1.01	7.0	2015	[47]
PBDT-TS1:PDIODT	Doctor-blading	*o*-MA	Glass/ITO	Thermal evap.	0.07	5.21	53.4	0.74	12.8	2016	[77]
PTzBI:N2200	Doctor-blading	MeTHF	Glass/ITO	Thermal evap.	0.04	8.36	66.7	0.84	14.9	2019	[78]
PBTA-TF:IT-M	Doctor-blading	THF:IP	Glass/ITO	Thermal evap.	0.04	11.70	66.0	0.95	18.1	2017	[79]
	Doctor-blading	THF:IP	Glass/ITO	Thermal evap.	1.00	10.60	65.0	0.95	17.1		

Table 1. (Continued.)

D:A materials (see figures 9–10)	Active layer deposition	Solvent(s)	Substrate	Top electrode deposition	Device area (cm^2)	PCE_{max} (%)	FF (%)	V_{oc} (V)	J_{sc} (mA cm^{-2})	Year	References
FTAZ:IT-M	Doctor-blading	Toluene	Glass/ITO	Thermal evap.	0.07	11.00	66.1	0.95	16.8	2018	[31]
	Doctor-blading	Toluene	Glass/ITO	Thermal evap.	0.56	9.80	64.6	0.93	16.4		
PTB7-Th:ITIC	Doctor-blading	CB:DIO	Glass/ITO	Thermal evap.	0.14	9.54	71.0	0.83	16.0	2018	[80]
	Doctor-blading	CB:DIO	PET	Thermal evap.	2.03	7.60	63.0	0.81	14.7		
PBDB-T:ITIC	Doctor-blading	CB:DIO	Glass/ITO	Thermal evap.	0.04	10.00	66.1	0.89	17.1	2018	[32]
PBDB-T:IT-4F	Doctor-blading	CB:DIO	Glass/ITO	Thermal evap.	0.12	12.88	72.0	0.86	20.8	2018	[83]
	Doctor-blading	CB:DIO	Glass/ITO	Thermal evap.	1.04	9.22	N/A	N/A	N/A		
P3HT:O-IDTBR	Doctor-blading	CB:*o*-DCB	Glass/ITO	Thermal evap.	0.08	5.60	61.6	0.74	12.4	2019	[84]
P3HT:O-IDTBR	Inkjet printing	*o*-DCB	Glass/ITO	Thermal evap.	0.10	6.47	67.2	0.71	13.8	2019	[85]
	Inkjet printing	*o*-DCB	Glass/ITO	Thermal evap.	2.00	6.00	N/A	N/A	N/A		
	Inkjet printing	*o*-DCB	Glass/ITO	Thermal evap.	2.20	4.76	47.0	0.72	14.1		
PBDB-TF:BTPTT-4F	Spin-coating	CF:CN	Glass/ITO	Thermal evap.	0.07	15.70	76.1	0.82	25.2	2019	[8]
P2F-Ehp:BTPTT-4F	Spin-coating	CF:DBE	Glass/ITO	Thermal evap.	0.05	16.00	74.1	0.82	26.7	2019	[87]
PDTB-EF-T:IT-4F	Spin-coating	CB:DIO	Glass/ITO	Thermal evap.	N/A	14.20	76.0	0.90	20.7	2018	[29]

[a]Average value of >10 cells; [a]characteristics measured over 0.12 cm^2 cells; CB: chlorobenzene, CN: 1-chloronaphthalene, CF: chloroform, *o*-DCB: 1,2-dichlorobenzene, BrA: 4-bromoanisole, *o*-MA: 2-methylanisole, (Me)THF: (2-methyl) tetrahydrofuran, IP: isopropanol, DBE: dibenzylether.

ITO, and green for ITO-free PET to indicate their scalability.

6. Conclusions and outlook

The field of organic solar cells has been moving fast in recent years, and record efficiencies are published regularly using new non-fullerene acceptor materials. In this perspective, we have sought to identify focus points for overcoming the challenge of upscaling the fabrication of organic solar cells based on these non-fullerene acceptors. By categorizing a wide range of deposition techniques in terms of their compatibility with continuous roll-to-roll setups, their material waste, and their throughput as either fully scalable, partly scalable, or non-scalable, the literature on fullerene-free OPVs was reviewed using these classifications. Although numerous studies have been published on laboratory-scale devices fabricated using non-scalable deposition techniques, only a small number have been published on devices fabricated using fully- or partly scalable deposition techniques. However, combining the knowledge gained from these few studies allows us to suggest three main priorities for meeting the lab-to-fab challenge.

(i) First of all, implementing dual temperature control, meaning that both the ink- and substrate temperatures can be controlled simultaneously and independently, for example through the use of heated slot-die coating heads, has shown to be an impressively effective way of optimizing the active layer morphologies, leading to some of the highest efficiencies published for flexible OPVs.

(ii) Secondly, the use of non-halogenated, i.e. 'green', solvents for active layer deposition has in several cases shown to be superior to using halogenated solvents. Some of these studies also point to the fact that processing additives, which are common in halogenated solvent formulations and which might cause device performance to deteriorate with time and illumination, can be made redundant with green solvents. Furthermore, tuning the boiling point of the active layer solvent formulation is crucial to facilitate preferential morphology evolution during evaporation when depositing active layers with scalable techniques. Systematic *in situ* studies can aid the interpretation of such studies.

(iii) Finally, the interfacial layers should be optimized for continuous deposition techniques. The well-performing systems with roll-to-roll deposited active layers and evaporated top electrodes reviewed in section 5.2 all utilize thermally evaporated MoO_3 hole-transport layers. As vacuum deposition, as discussed, could very well be connected to high processing costs, solution processable formulations of molybdenum oxide hole-transport layers have great potential as replacements of thermally evaporated MoO_3 layers [88], whereas also solution processable molybdenum sulfide hole-transport layers show promise with performance comparable to PEDOT:PSS-based devices [89]. Very recently, solution processed tungsten sulfide layers have also shown great promise as hole-transport layers [90]. We thus recommend that improving solution processed interfacial layers is prioritized going forward, as significant efficiency gains for scalably fabricated, flexible organic solar cells are expected if the qualities of solution processed charge transport layers can get close to the ones of the evaporated. In addition, the interface between the electron-transport layer, usually ZnO nanoparticles, and the active layer has shown to be important too as reviewed in section 5.3. Simply by changing the processing solvent, a higher smoothness and fewer voids and inhomogeneities can be achieved in spin-coated ZnO layers, in turn leading to relative efficiency increases of almost 10% for devices with blade-coated active layers [84]. Studying the surface morphology of these interfacial layers with varying processing conditions when deposited using fully scalable methods is thus important going forward, as the optimal conditions might differ significantly from the spin-coated ones.

If these three points are addressed, we are confident that the 10-10 goals of 10% efficiency and 10 years stability for scalably fabricated organic solar cells can be reached [1, 7, 24], making sustainable, large-scale fabrication viable. We urge that large-area devices (>1 cm^2) fabricated using scalable deposition techniques are reported alongside the laboratory-scale champion devices, preferably accompanied by stability analyses, in order to move towards these goals and identify promising material systems for upscaling.

Acknowledgments

We acknowledge financial support from the H2020 European Research Council through the SEEWHI Consolidator grant, ERC-2015-CoG-681881.

Conflicts of interest

There are no conflicts of interest to report.

ORCID iDs

Anders S Gertsen https://orcid.org/0000-0002-4712-0339
Marcial Fernández Castro https://orcid.org/0000-0003-3294-2994

Roar R Søndergaard https://orcid.org/0000-0003-3567-3400
Jens W Andreasen https://orcid.org/0000-0002-3145-0229

References

[1] Søndergaard R, Hösel M, Angmo D, Larsen-Olsen T T and Krebs F C 2012 Roll-to-roll fabrication of polymer solar cells *Mater. Today* **15** 36–49
[2] Lucera L, Kubis P, Fecher F W, Bronnbauer C, Turbiez M, Forberich K, Ameri T, Egelhaaf H and Brabec C J 2015 Guidelines for closing the efficiency gap between hero solar cells and roll-to-roll printed modules *Energy Technol.* **3** 373–84
[3] Gu X *et al* 2017 Roll-to-roll printed large-area all-polymer solar cells with 5% efficiency based on a low crystallinity conjugated polymer blend *Adv. Energy Mater.* **7** 1602742
[4] Espinosa N, Hosel M, Angmo D and Krebs F C 2012 Solar cells with one-day energy payback for the factories of the future *Energy Environ. Sci.* **5** 5117–32
[5] Peng J, Lu L and Yang H 2013 Review on life cycle assessment of energy payback and greenhouse gas emission of solar photovoltaic systems *Renew. Sustain. Energy Rev.* **19** 255–74
[6] Emmott C J, Urbina A and Nelson J 2012 Environmental and economic assessment of ITO-free electrodes for organic solar cells *Sol. Energy Mater. Sol. Cells* **97** 14–21
[7] Gambhir A, Sandwell P and Nelson J 2016 The future costs of OPV—A bottom-up model of material and manufacturing costs with uncertainty analysis *Sol. Energy Mater. Sol. Cells* **156** 49–58
[8] Yuan J *et al* 2019 Single-junction organic solar cell with over 15% efficiency using fused-ring acceptor with electron-deficient core *Joule* **3** 1140-51
[9] Lin Y and Zhan X 2014 Non-fullerene acceptors for organic photovoltaics: an emerging horizon *Mater. Horiz.* **1** 470–88
[10] Lin Y, Wang J, Zhang Z-G, Bai H, Li Y, Zhu D and Zhan X 2015 An electron acceptor challenging fullerenes for efficient polymer solar cells *Adv. Mater.* **27** 1170–4
[11] Cheng P, Bai H, Zawacka N K, Andersen T R, Liu W, Bundgaard E, Jørgensen M, Chen H, Krebs F C and Zhan X 2015 Roll-coated fabrication of fullerene-free organic solar cells with improved stability *Adv. Sci.* **2** 1500096
[12] Gasparini N *et al* 2017 Burn-in free nonfullerene-based organic solar cells *Adv. Energy Mater.* **7** 1700770
[13] Cha H *et al* 2017 An efficient, 'burn in' free organic solar cell employing a nonfullerene electron acceptor *Adv. Mater.* **29** 1701156
[14] Zhang G, Zhao J, Chow P C Y, Jiang K, Zhang J, Zhu Z, Zhang J, Huang F and Yan H 2018 Nonfullerene acceptor molecules for bulk heterojunction organic solar cells *Chem. Rev.* **118** 3447–507
[15] Cheng P, Li G, Zhan X and Yang Y 2018 Next-generation organic photovoltaics based on non-fullerene acceptors *Nat. Photon.* **12** 131–42
[16] Du X, Heumueller T, Gruber W, Classen A, Unruh T, Li N and Brabec C J 2019 Efficient polymer solar cells based on non-fullerene acceptors with potential device lifetime approaching 10 years *Joule* **3** 215–26
[17] Fan Q *et al* 2018 High-performance as-cast nonfullerene polymer solar cells with thicker active layer and large area exceeding 11% power conversion efficiency *Adv. Mater.* **30** 1704546
[18] Wang N, Yang W, Li S, Shi M, Lau T-K, Lu X, Shikler R, Li C-Z and Chen H 2019 A non-fullerene acceptor enables efficient P3HT-based organic solar cells with small voltage loss and thickness insensitivity *Chin. Chem. Lett.* **30** 1277–81
[19] Krebs F C, Gevorgyan S A and Alstrup J 2009 A roll-to-roll process to flexible polymer solar cells: model studies, manufacture and operational stability studies *J. Mater. Chem.* **19** 5442–51
[20] Li N *et al* 2013 Towards 15% energy conversion efficiency: a systematic study of the solution-processed organic tandem solar cells based on commercially available materials *Energy Environ. Sci.* **6** 3407–13
[21] Burgués-Ceballos I, Stella M, Lacharmoise P and Martínez-Ferrero E 2014 Towards industrialization of polymer solar cells: material processing for upscaling *J. Mater. Chem.* A **2** 17711–22
[22] Po R, Bernardi A, Calabrese A, Carbonera C, Corso G and Pellegrino A 2014 From lab to fab: how must the polymer solar cell materials design change? An industrial perspective *Energy Environ. Sci.* **7** 925–43
[23] Min J, Luponosov Y N, Cui C, Kan B, Chen H, Wan X, Chen Y, Ponomarenko S A, Li Y and Brabec C J 2017 Evaluation of electron donor materials for solution-processed organic solar cells via a novel figure of merit *Adv. Energy Mater.* **7** 1700465
[24] Azzopardi B, Emmott C J M, Urbina A, Krebs F C, Mutale J and Nelson J 2011 Economic assessment of solar electricity production from organic-based photovoltaic modules in a domestic environment *Energy Environ. Sci.* **4** 3741–53
[25] Bin H *et al* 2016 11.4% efficiency non-fullerene polymer solar cells with trialkylsilyl substituted 2D-conjugated polymer as donor *Nat. Commun.* **7** 13651
[26] Li S, Ye L, Zhao W, Zhang S, Mukherjee S, Ade H and Hou J 2016 Energy-level modulation of small-molecule electron acceptors to achieve over 12% efficiency in polymer solar cells *Adv. Mater.* **28** 9423–9
[27] Zhao W, Li S, Yao H, Zhang S, Zhang Y, Yang B and Hou J 2017 Molecular optimization enables over 13% efficiency in organic solar cells *J. Am. Chem. Soc.* **139** 7148–51
[28] Zhang S, Qin Y, Zhu J and Hou J 2018 Over 14% efficiency in polymer solar cells enabled by a chlorinated polymer donor *Adv. Mater.* **30** 1800868
[29] Li S, Ye L, Zhao W, Yan H, Yang B, Liu D, Li W, Ade H and Hou J 2018 A wide band gap polymer with a deep highest occupied molecular orbital level enables 14.2% efficiency in polymer solar cells *J. Am. Chem. Soc.* **140** 7159–67
[30] Zheng Z *et al* 2018 A highly efficient non-fullerene organic solar cell with a fill factor over 0.80 enabled by a fine-tuned hole-transporting layer *Adv. Mater.* **30** 1801801
[31] Ye L, Xiong Y, Zhang Q, Li S, Wang C, Jiang Z, Hou J, You W and Ade H 2018 Surpassing 10% efficiency benchmark for nonfullerene organic solar cells by scalable coating in air from single nonhalogenated solvent *Adv. Mater.* **30** 1705485
[32] Zhang L, Lin B, Hu B, Xu X and Ma W 2018 Blade-cast nonfullerene organic solar cells in air with excellent morphology, efficiency, and stability *Adv. Mater.* **30** 1800343
[33] Na S-I *et al* 2019 High performance roll-to-roll produced fullerene-free organic photovoltaic devices via temperature-controlled slot die coating *Adv. Funct. Mater.* **29** 1805825
[34] Huang Y-C, Cha H-C, Chen C-Y and Tsao C-S 2017 A universal roll-to-roll slot-die coating approach towards high-efficiency organic photovoltaics *Prog. Photovolt.* **25** 928–35
[35] Swartwout R, Hoerantner M T and Bulovic V 2019 Scalable deposition methods for large-area production of perovskite thin films *Energy Environ. Mater.* **2** 119–43
[36] Li N, McCulloch I and Brabec C J 2018 Analyzing the efficiency, stability and cost potential for fullerene-free organic photovoltaics in one figure of merit *Energy Environ. Sci.* **11** 1355–61
[37] Bundgaard E *et al* 2015 Matrix organization and merit factor evaluation as a method to address the challenge of finding a polymer material for roll coated polymer solar cells *Adv. Energy Mater.* **5** 1402186
[38] Benten H, Mori D, Ohkita H and Ito S 2016 Recent research progress of polymer donor/polymer acceptor blend solar cells *J. Mater. Chem.* A **4** 5340–65
[39] Yan C, Barlow S, Wang Z, Yan H, Jen A K, Marder S R and Zhan X 2018 Non-fullerene acceptors for organic solar cells *Nat. Rev. Mater.* **3** 18003
[40] Sun H, Chen F and Chen Z-K 2019 Recent progress on non-fullerene acceptors for organic photovoltaics *Mater. Today* **24** 94–118
[41] Espinosa N, Garc-Valverde R, Urbina A and Krebs F C 2011 A life cycle analysis of polymer solar cell modules prepared using

roll-to-roll methods under ambient conditions *Sol. Energy Mater. Sol. Cells* **95** 1293–302
[42] Espinosa N, Garc-Valverde R, Urbina A, Lenzmann F, Manceau M, Angmo D and Krebs F C 2012 Life cycle assessment of ITO-free flexible polymer solar cells prepared by roll-to-roll coating and printing *Sol. Energy Mater. Sol. Cells* **97** 3–13
[43] Tsang M P, Sonnemann G W and Bassani D M 2016 Life-cycle assessment of cradle-to-grave opportunities and environmental impacts of organic photovoltaic solar panels compared to conventional technologies *Sol. Energy Mater. Sol. Cells* **156** 37–48
[44] Krebs F C 2009 Fabrication and processing of polymer solar cells: a review of printing and coating techniques *Sol. Energy Mater. Sol. Cells* **93** 394–412
[45] Roth B, Søndergaard R and Krebs F 2015 Roll-to-roll printing and coating techniques for manufacturing large-area flexible organic electronics *Handbook of Flexible Organic Electronics* ed S Logothetidis (Oxford: Woodhead Publishing) ch 7 pp 171–97
[46] Diao Y *et al* 2013 Solution coating of large-area organic semiconductor thin films with aligned single-crystalline domains *Nat. Mater.* **12** 665
[47] Diao Y *et al* 2015 Flow-enhanced solution printing of all-polymer solar cells *Nat. Commun.* **6** 7955
[48] Gu X, Shaw L, Gu K, Toney M F and Bao Z 2018 The meniscus-guided deposition of semiconducting polymers *Nat. Commun.* **9** 534
[49] Song S, Lee K T, Koh C W, Shin H, Gao M, Woo H Y, Vak D and Kim J Y 2018 Hot slot die coating for additive-free fabrication of high performance roll-to-roll processed polymer solar cells *Energy Environ. Sci.* **11** 3248–55
[50] Aziz F and Ismail A 2015 Spray coating methods for polymer solar cells fabrication: a review *Mater. Sci. Semicond. Process.* **39** 416–25
[51] Andersen T R *et al* 2014 Scalable, ambient atmosphere roll-to-roll manufacture of encapsulated large area, flexible organic tandem solar cell modules *Energy Environ. Sci.* **7** 2925–33
[52] Brandt R G, Zhang F, Andersen T R, Angmo D, Shi M, Gurevich L, Krebs F C, Andreasen J W and Yu D 2016 Roll coated large area ITO- and vacuum-free all organic solar cells from diketopyrrolopyrrole based non-fullerene acceptors with molecular geometry effects *RSC Adv.* **6** 41542–50
[53] Carlé J E *et al* 2017 Overcoming the scaling lag for polymer solar cells *Joule* **1** 274–89
[54] Heliatek, 'About Heliatek.' https://heliatek.com/en/heliatek/about-us (Accessed: 30 April, 2019)
[55] Destouesse E, Top M, Lamminaho J, Rubahn H, Fahlteich J and Madsen M 2019 Slot-die processing and encapsulation of non-fullerene based ito-free organic solar cells and modules *Flex. Print. Electron.* **4** 045004
[56] He Y and Li Y 2011 Fullerene derivative acceptors for high performance polymer solar cells *Phys. Chem. Chem. Phys.* **13** 1970–83
[57] Lin Y *et al* 2016 High-performance electron acceptor with thienyl side chains for organic photovoltaics *J. Am. Chem. Soc.* **138** 4955–61
[58] Dai S *et al* 2017 Fused nonacyclic electron acceptors for efficient polymer solar cells *J. Am. Chem. Soc.* **139** 1336–43
[59] Zhan X, Tan Z, Domercq B, An Z, Zhang X, Barlow S, Li Y, Zhu D, Kippelen B and Marder S R 2007 A high-mobility electron-transport polymer with broad absorption and its use in field-effect transistors and all-polymer solar cells *J. Am. Chem. Soc.* **129** 7246–7
[60] Genene Z, Mammo W, Wang E and Andersson M R 2019 Recent advances in n-type polymers for all-polymer solar cells *Adv. Mater.* **31** 1807275
[61] Strohm S, Machui F, Langner S, Kubis P, Gasparini N, Salvador M, McCulloch I, Egelhaaf H-J and Brabec C J 2018 P3HT: non-fullerene acceptor based large area, semi-transparent PV modules with power conversion efficiencies of 5%, processed by industrially scalable methods *Energy Environ. Sci.* **11** 2225–34
[62] Lin Y *et al* 2018 Printed nonfullerene organic solar cells with the highest efficiency of 9.5% *Adv. Energy Mater.* **8** 1701942
[63] Corzo D, Almasabi K, Bihar E, Macphee S, Rosas-Villalva D, Gasparini N, Inal S and Baran D 2019 Digital inkjet printing of high-efficiency large-area nonfullerene organic solar cells *Adv. Mater. Technol.* **4** 1900040
[64] Liu Y, Larsen-Olsen T T, Zhao X, Andreasen B, Søndergaard R R, Helgesen M, Norrman K, Jørgensen M, Krebs F C and Zhan X 2013 All polymer photovoltaics: from small inverted devices to large roll-to-roll coated and printed solar cells *Sol. Energy Mater. Sol. Cells* **112** 157–62
[65] Angmo D and Krebs F C 2013 Flexible ITO-free polymer solar cells *J. Appl. Polym. Sci.* **129** 1–14
[66] Roth B, Benatto G A d R, Corazza M, Carlé J E, Helgesen M, Gevorgyan S A, Jørgensen M, Søndergaard R R and Krebs F C 2016 Improving the operational stability of PBDTTTz-4 polymer solar cells modules by electrode modification *Adv. Eng. Mater.* **18** 511–7
[67] Chen M-R, Fan C-C, Andersen T R, Dam H F, Fu W-F, Lin Y-Z, Bundgaard E, Krebs F C, Zhan X-W and Chen H-Z 2014 Solvent-resistant small molecule solar cells by roll-to-roll fabrication via introduction of azide cross-linkable group *Synth. Met.* **195** 299–305
[68] Dam H F and Krebs F C 2012 Simple roll coater with variable coating and temperature control for printed polymer solar cells *Sol. Energy Mater. Sol. Cells* **97** 191–6
[69] Carlé J E, Andersen T R, Helgesen M, Bundgaard E, Jørgensen M and Krebs F C 2013 A laboratory scale approach to polymer solar cells using one coating/printing machine, flexible substrates, no ITO, no vacuum and no spincoating *Sol. Energy Mater. Sol. Cells* **108** 126–8
[70] Cheng P, Lin Y, Zawacka N K, Andersen T R, Liu W, Bundgaard E, Jørgensen M, Chen H, Krebs F C and Zhan X 2014 Comparison of additive amount used in spin-coated and roll-coated organic solar cells *J. Mater. Chem.* A **2** 19542–9
[71] Liu K, Larsen-Olsen T T, Lin Y, Beliatis M, Bundgaard E, Jørgensen M, Krebs F C and Zhan X 2016 Roll-coating fabrication of flexible organic solar cells: comparison of fullerene and fullerene-free systems *J. Mater. Chem.* A **4** 1044–51
[72] Rossander L H, Zawacka N K, Dam H F, Krebs F C and Andreasen J W 2014 *In situ* monitoring of structure formation in the active layer of polymer solar cells during roll-to-roll coating *AIP Adv.* **4** 087105
[73] Zawacka N K, Andersen T R, Andreasen J W, Rossander L H, Dam H F, Jorgensen M and Krebs F C 2014 The influence of additives on the morphology and stability of roll-to-roll processed polymer solar cells studied through ex situ and *in situ* X-ray scattering *J. Mater. Chem.* A **2** 18644–54
[74] Richter L J, DeLongchamp D M and Amassian A 2017 Morphology development in solution-processed functional organic blend films: an *in situ* viewpoint *Chem. Rev.* **117** 6332–66
[75] Rossander L H, Dam H F, Carle J E, Helgesen M, Rajkovic I, Corazza M, Krebs F C and Andreasen J W 2017 In-line, roll-to-roll morphology analysis of organic solar cell active layers *Energy Environ. Sci.* **10** 2411–9
[76] Baran D *et al* 2016 Reduced voltage losses yield 10% efficient fullerene free organic solar cells with >1 V open circuit voltages *Energy Environ. Sci.* **9** 3783–93
[77] Baran D *et al* 2017 Reducing the efficiency-stability-cost gap of organic photovoltaics with highly efficient and stable small molecule acceptor ternary solar cells *Nat. Mater.* **16** 363–70
[78] Wadsworth A *et al* 2017 Highly efficient and reproducible nonfullerene solar cells from hydrocarbon solvents *ACS Energy Lett.* **2** 1494–500
[79] Ye L *et al* 2016 High performance organic solar cells processed by blade coating in air from a benign food additive solution *Chem. Mater.* **28** 7451–8
[80] Lin B *et al* 2019 Molecular packing control enables excellent performance and mechanical property of blade-cast all-polymer solar cells *Nano Energy* **59** 277–84

[81] Zhao W, Zhang S, Zhang Y, Li S, Liu X, He C, Zheng Z and Hou J 2018 Environmentally friendly solvent-processed organic solar cells that are highly efficient and adaptable for the blade-coating method *Adv. Mater.* **30** 1
[82] Kim W, Kim J K, Kim E, Ahn T K, Wang D H and Park J H 2015 Conflicted effects of a solvent additive on ptb7:pc71bm bulk heterojunction solar cells *J. Phys. Chem.* C **119** 5954–61
[83] Jacobs I E, Wang F, Bedolla Valdez Z I, Ayala Oviedo A N, Bilsky D J and Moulé A J 2018 Photoinduced degradation from trace 1, 8-diiodooctane in organic photovoltaics *J. Mater. Chem.* C **6** 219–25
[84] Ji G, Zhao W, Wei J, Yan L, Han Y, Luo Q, Yang S, Hou J and Ma C-Q 2019 12.88% efficiency in doctor-blade coated organic solar cells through optimizing the surface morphology of a ZnO cathode buffer layer *J. Mater. Chem.* A **7** 212–20
[85] Pascual-San-José E, Rodrez-Martínez X, Adel-Abdelaleim R, Stella M, Martínez-Ferrero E and Campoy-Quiles M 2019 Blade coated P3HT:non-fullerene acceptor solar cells: a high-throughput parameter study with a focus on up-scalability *J. Mater. Chem.* A **7** 20369–82
[86] Tan M J, Zhong S, Li J, Chen Z and Chen W 2013 Air-stable efficient inverted polymer solar cells using solution-processed nanocrystalline ZnO interfacial layer *ACS Appl. Mater. Interfaces* **5** 4696–701
[87] Fan B, Zhang D, Li M, Zhong W, Zeng Z, Ying L, Huang F and Cao Y 2019 Achieving over 16% efficiency for single-junction organic solar cells *Sci. China Chem.* **62** 746–52
[88] Yi Q *et al* 2015 Aqueous solution-deposited molybdenum oxide films as an anode interfacial layer for organic solar cells *ACS Appl. Mater. Interfaces* **7** 18218–24
[89] Wei J, Yin Z, Chen S-C, Cai D and Zheng Q 2016 Solution-processed MoSx thin-films as hole-transport layers for efficient polymer solar cells *RSC Adv.* **6** 39137–43
[90] Lin Y *et al* 2019 17% efficient organic solar cells based on liquid exfoliated WS2 as a replacement for PEDOT:PSS *Adv. Mater.* **31** 1902965